Individual-based modeling of mangrove forest growth: MesoFON – Recent calibration and future direction

Uwe Grueters[a,*,1], Mohd Rodila Ibrahim[b,1], Behara Satyanarayana[b], Farid Dahdouh-Guebas[c,d]

[a] Dendro-Institute Tharandt, Dresden University of Technology (TU Dresden), Pienner Strasse 8, D-01737, Tharandt, Germany
[b] Mangrove Research Unit (MARU), Institute of Oceanography and Environment (INOS), University Malaysia Terengganu - UMT, Kuala Terengganu, Malaysia
[c] Laboratory of Systems Ecology and Resource Management, Department of Organism Biology, Université Libre de Bruxelles – ULB, Av. F.D. Roosevelt 50, CPI 264/1, B-1050, Brussels, Belgium
[d] Laboratory of Plant Biology and Nature Management, Department of Biology, Vrije Universiteit Brussel – VUB, Pleinlaan 2, B-1050, Brussels, Belgium

ARTICLE INFO

ABSTRACT

We introduce individual-based models (IBMs) of mangrove forests and criticize the tasks for their development recommended previously for being mostly related to natural threats. This is contrasted with our perspective that the key research question of today's models should be to mitigate anthropogenic threats.

Core objective (1) of this article is to provide a review of mangrove threats prioritizing solution-oriented IBM approaches. Because species-specific calibration of IBMs is time-consuming, efficiency is crucial. Globally, we identify an urgent need to parametrize Asian mangrove species.

We suggest IBMs to unveil management scenarios with maximum sustainable timber yield to prevent mangrove conversion and over-exploitation. The key model purpose regarding natural threats is to govern the management of mangrove forest stability for coastal protection using a combination of windthrow models and IBMs. We argue for the embedding of IBMs in ecosystem models to achieve purposes regarding eutrophication and altered hydrology/sedimentation.

Core objective (2) is to describe the development of the new IBM mesoFON from a task-to a solution-oriented model. Initially, the interaction of lateral crown displacement and hurricane impacts was examined with mesoFON. Later, we introduced propagule production & local dispersal with the task to close the tree life cycle. Here, we describe the change in purpose of mesoFON accompanying its calibration for *Rhizophora apiculata* in Malaysia. For this we applied a Genetic Algorithm optimizer, used mesoFON as a "way-back machine", initialized it with observed tree diameters/positions and shrank the trees backwards in time.

Objective(3) is to describe mesoFON's future direction: Embedding in the General Ecosystem Model (Fitz et al., 1996) and targeting the solution of threats at larger spatial scales. Finally, we demonstrate that the new model simulates overland waterflow qualitatively right even in benchmark settings.

"Where this sort of Tree grows, it is impossible to march, by reason of these Stakes, which grow so mixt one amongst another, that I have, when forced to go thro' them, gone half a mile, and never set my foot on the Ground, stepping from Root to Root." (William Dampier: A New Voyage Round the World. Page 54, Publisher: J. Knapton, 1699)

1. Introduction

How better to illustrate the structural richness of the mangrove than with this historical description of a red mangrove forest, taken from the travel narrative of William Dampier, the British buccaneer and explorer. Mangroves are natural forests along tropical coastlines with uneven-aged trees and multi-layered structure formed by demographic processes. They are shaped by the freshwater streaming into the ecotone and by the physical forces of the ever-returning tides, tropical storms and floods. Moreover, mangrove forests are oligo- or even multi-specific, the latter particularly in the Indo-West-Pacific.

1.1. Development of mangrove modeling

Mangroves - like other natural forests - are not the mono-specific,

---

Table 1
Tasks for individual-based models of mangrove forest dynamics from verbal descriptions of Berger et al. (2008) in a slightly abridged version.

Tasks	Individual-based models of mangrove forests should..
Task 1	describe the essential life processes of trees linked to resource, regulator and hydroperiod gradients
Task 2	test the impact of changes in disturbance regimes on mangrove forest dynamics
Task 3	evaluate different management scenarios according to their potential ecological, economic, or social outcome of mangrove sustainability
Task 4	compare recovery patterns to test the plausibility of different hypotheses explaining the role of resource gradients in mangrove gaps
Task 5	synthesize the species-specific and age-specific regeneration potential of individual trees after disturbances and their importance for forest recovery
Task 6	contribute to understanding the roles and relative contribution of inter-specific competition and "chance" in structuring mangrove forests following gap formation
Task 7	test the synchronization and de-synchronization effect of canopy disturbances on mosaic cycles of successional forest stages on a landscape level to develop a general understanding of mangrove forest dynamics

even-aged type of forest plantations the developers of traditional forest growth modeling tools, such as yield tables, had in mind for more than 200 years (Pretzsch, 2009; Weiskittel, 2011). Hence, it is quite understandable that models for mangrove forests, in comparison, appeared rather late, since techniques for the (empirical) modeling of uneven-aged stands, both, whole stand and size-class models, did not become available until the second half of the 1960s (Burkhart and Tomé, 2012).

Burns and Ogden (1985) were the first who applied a size-class model to mangrove forests. The authors simulated the transition of diameter size classes in *Avicennia marina* (Forssk.) Vierh. stands using the Leslie matrix approach.

But mangrove forest modeling has benefitted much more from the development of individual tree growth and yield models in the form of successional forest gap models (see Pretzsch, 2009 for an overview of these approaches). JABOWA from Botkin et al. (1972) can be considered as the prototype for this kind of models. The gap, a small grid cell of the size of an individual mature tree (usually 10 m × 10 m wide), is the unit of information/computation in these models. The term "gap" is used because grid cells could be either occupied by a closed canopy or free from vegetation, thereby forming a mosaic on the landscape. The maximum growth inside a grid cell is given by an optimum growth function. Unfavorable environmental conditions in terms of radiation, temperature, soil fertility and water availability reduce growth multiplicatively from the optimum. Successors of JABOWA, mainly variants of the FORET model, were applied to large numbers of species in many forest regions and their usage was raised almost to the global level by Shugart (1984). The next class of gap models was the SORTIE model (Pacala et al., 1993), in which the Monsi and Saeki (1953) approach to determine the radiation available to the canopy was replaced by a data-driven and more individual-based approach to determine the growth reduction by light (Canham et al., 1994). With 126 official publications (SORTIE-ND, (c) 2001–2017) and more than 15,000 citations (according to Google, Google Scholar) SORTIE has become one of the most widely used and best-known individual-based models of forest dynamics. Who has not watched the fascinating animations, published by Deutschman et al. (1997) on Science Online, in which partial and complete circular clear-cuts were recolonized? Partial clear-cuts were first rapidly filled by the fast-growing light-requiring species, later being overgrown by shade-tolerant species until finally the original state of the base-line (climax) forest was restored. In contrast, climax tree species, due to their restricted seed dispersal, were not able to recolonize complete clear-cuts. Deutschman et al. (1997) point out improvements in terms of recruitment being made in the transition of models: In JABOWA recruits are drawn from a predetermined, external list of species; unlike, in the FORET class of models seedlings are produced by the adult trees, but are often dispersed globally on the landscape; only in SORTIE the seedlings are dispersed localized around parental trees. As described above, these alterations had substantial consequences on simulated community dynamics.

Coming back to the benefits of these approaches for mangrove research: Most recently Berger et al. (2008) reviewed the status of mangrove IBMs and identified primary tasks for the future development of such models. At that time, three IBMs were available: FORMAN (Chen and Twilley, 1998), KiWi (Berger and Hildenbrandt, 2000) and MANGRO (Doyle et al., 1995). While FORMAN is a JABOWA type of model, MANGRO is a derivative of a FORET variant (Doyle, 1981), and even KiWi retains major components of the JABOWA model. The purpose of all three IBMs is to simulate mangrove community dynamics comprised of *Rhizophora mangle* L.*, Avicennia germinans* (L.) Stearns. and *Laguncularia racemosa* (L.) Gaertn.f. in the Neotropics. Regions of application have varied considerably among the models (MANGRO: Everglades, FL; FORMAN: FL, LA, Colombia; KiWi with a general focus on theoretical questions: Brazil, Belize, but also for *Rhizophora apiculata* Bl. in Malaysia (Fontalvo-Herazo et al., 2011) and Viet Nam (Kautz et al., 2011)). All three models simulate tree recruitment as saplings (or seedlings in case of MANGRO), growth constrained by environmental conditions as in JABOWA (additionally including salinity) and tree mortality. A major difference among the models is: MANGRO and FORMAN are integrated in landscape models, whereas KiWi is not and operates merely at the stand level. While MANGRO uses SELVA (Doyle et al., 2003) to simulate hydrological dynamics at the landscape scale, FORMAN uses HYMAN (hydrology model, Twilley and Chen, 1998), NUMAN (nutrients model, Chen and Twilley, 1999) and SALSA (salinity box model, Twilley and Rivera-Monroy, 2005), respectively, to simulate large-scale hydrological and biogeochemical dynamics. MANGRO is unique in terms of recruitment: Trees establish as seedlings in dependence on site elevation, tidal flooding and species composition of stands in the neighborhood. KiWi is special in its way to simulate a tree's interaction with neighbors via a flexible competition index, the field-of-neighborhood (FON).

1.2. Tasks for mangrove IBMs and its critique

Primary tasks for the future development of mangrove IBMs consensually formulated by all main developers of such models (Berger et al., 2008) are listed in a slightly abridged version in Table 1.

Task 1 is certainly the most fundamental. IBMs are defined by the criteria: reflection of an individual's life cycle, resource dynamics, variability among individuals (Grimm and Railsback, 2005). Following this, mangrove IBMs should describe the essential life processes of trees linked to resources (carbon, nitrogen and phosphorus), regulators (salt, redox potential, and sulfide level) and hydro-period gradients. The disturbance experiments of Deutschman et al. (1997) are an illustrative example of how important the inclusion of all essential life processes in forest-growth IBMs is.

Tasks 2,4,5,6 are all related to effects of disturbance regime on community dynamics. Natural disturbance events, such as hurricane and lightning impacts, represent local threats at the stand level (compare Piou et al., 2008; Vogt et al., 2014; Grueters et al., 2014). Yet, the main focus on the natural threat of disturbance does not appear adequate given the plethora of anthropogenic threats that have led to the massive global mangrove loss (Valiela et al., 2001; Duke et al., 2007). Task 3 is the only one that covers an anthropogenic threat, i.e. over-exploitation and the sustainability of mangrove management. Task 7, the association of disturbance regime with the mosaic cycle is the only one that targets processes on a larger spatial scale. This is unfortunate,

because various anthropogenic threats affect the whole mangrove ecotone. Those effects can only be simulated by IBMs that are integrated in large landscape models, such as FORMAN and MANGRO (compare section 1.1).

The primary objective of all ecological modeling is to solve problems or answer questions (Grimm and Railsback, 2005, p. 22). In our opinion, the key research question of today should be to mitigate specific anthropogenic threats to mangroves. Hence, our main criticism of these tasks is that (except for task 3) this research question is lacking from them.

1.3. Aim of this article

The core objectives of this article are (1) to provide a focused review of mangrove threats prioritizing solution-oriented IBM approaches, (2) to describe the calibration of the new IBM mesoFON and its development from a task-oriented to a solution-oriented individual-based mangrove growth model and (3) to derive a potential future direction for the mesoFON model targeting the solution of mangrove threats at larger spatial scales.

2. A review of mangrove threats and respective IBM purposes

Because species-specific model calibration requires large data sets and is very time-consuming, efficiency is crucial. A review of mangrove threats with the aim of prioritizing purposes of solution-oriented IBMs must concentrate on regions that have large mangrove coverage, tree species richness and high potential of (aboveground) biomass production and ecosystem carbon sequestration to mitigate climate change (Taillardat et al., 2018). Furthermore, the review must focus on important species in terms of distribution range, dominance and/or economic value. We therefore begin our review with a spatial analysis of the earth's mangroves. Relevant regions determine the variety of threats and related specific model purposes which we will discuss. Advantages/disadvantages of IBM applications are described, if a certain threat has been studied with the help of mangrove IBMs. Otherwise, certain limitations of IBMs are identified and more suitable model types are recommended.

2.1. Methodology of the review

First, we have assembled an overview of continental/regional mangrove coverages and threats based on the database of Hamilton and Casey (2016) and the FAO report of the world's mangroves (FAO, 2007, along with country profiles). Because the functioning of certain threats is somewhat obscure we have then linked threats with driving processes (or short drivers), such as Altered Hydrology (AltHyd), Salinization (Sal), Clear Felling (CF), Gap Formation (GF), Oligo- (Olig) or Eutrophication (Eut), Pollution (Poll) and Altered Sedimentation ($\pm$ Sed).

Finally, each threat is associated with one or more model types (IBM, MWM = Mechanistic Windthrow Model, FSM = Functional-Structural Model, EM = Ecosystem Model) that we consider to be suitable for the simulation of the threat. These model types are defined here as follows:

1. The IBM model type is defined by four criteria: reflection of an individual tree's life cycle, resource (regulator and hydrologic) dynamics, tree population sizes represented by integer numbers and variability among tree individuals (Grimm and Railsback, 2005).
2. The mechanistic wind-throw model type (MWM) estimates the risk of individual trees for uprooting or stem breakage based on tree attributes (species membership, crown width/height, stem diameter/height, wood density) and environmental factors, such as wind speed, tree density, distance from stand edge and soil type (Gardiner et al., 2000; Peltola et al., 1999).
3. The functional-structural model type (FSM) embraces the eco-

physiological processes of the tree organs (carbon allocation, photosynthesis, transpiration, respiration) and the 3d-architecture of branches (Godin and Sinoquet, 2005). FSMs are either single tree growth models (e.g. LIGNUM, Perttunen, 2008) or stand growth models (e.g. ALMIS, Eschenbach, 2005) and can be considered also as IBMs if they satisfy the above criteria.

4. The ecosystem model type (EM) encompasses the hydrology of a site (including H_2O input by precipitation, H_2O losses by transpiration and evaporation), the nutrient cycling of a site (including litter fall, decay of organic matter in the soil) and the lateral transport of water and suspended substances. Apparently, mangrove IBMs, such as FORMAN and MANGRO, that are integrated in landscape process models cover most components of ecosystem models.

2.2. Implications of the spatial analysis

Globally mangroves covered an area of $81.575\,km^2$ in 2014 (Hamilton and Casey, 2016). Almost half of that area is located in Asia ($38,195\,km^2$) and more than a quarter of the global area ($23,179\,km^2$) is found in Indonesia alone. Asia is not only of disproportionally high global relevance because of its huge mangrove area, but also because it is a region with the highest richness of mangrove tree species (Spalding et al., 2011), highest above-ground biomass of mangrove forests (Hutchison et al., 2014) and highest carbon sequestration in below-ground biomass and soil (Alongi, 2012; Sanderman et al., 2018). The results of our analysis can be found in Table A1 in Appendix A. It contains verbal descriptions of mangrove threats for regions/continents and most important countries, both ranked in descending order of mangrove coverage.

We identify an urgent need for efforts to parameterize the salinity- and nutrient-dependent tree growth functions underlying IBMs for Asian mangrove species. So far, the tall-stilt mangrove (*Rhizophora apiculata*) is the only Asian mangrove species for which parameters to use in IBMs are available (Fontalvo-Herazo et al., 2011; Kautz et al., 2011), but we consider those to be rather rough estimates.

Considering the results of the spatial analysis we decided to focus mainly on threats to Asian mangroves.

2.3. Threats to mangroves

As summarized in Fig. 1, we have classified the threats as Interior Threats (ch. 2.3.1) differentiating further between Anthropogenic Threats and Natural Threats, Up-stream Threats (ch. 2.3.2) and Downstream Threats (ch. 2.3.3).

2.3.1. Interior threats
2.3.1.1. Anthropogenic threats. **Conversion to other land uses:** According to FAO (2007) the first interior anthropogenic threat to Asian mangroves is conversion to shrimp farms, agriculture, salt pans and conversion due to urban, industrial and infrastructure development as well as tourism development. Currently, conversion to oil palm plantations is rising in importance (Richards and Friess, 2016; Feller et al., 2017).

Conversion to other land uses follows economic decisions made by local stakeholders in accordance with economic development plans devised by regional decision-makers. It is influenced by the estimated value of ecosystem services provided by mangrove forests. Among those, forestry products frequently provide the highest economic value (Salem and Mercer, 2012). Hence, the purpose of IBMs shall be to unveil management scenarios with maximum sustainable timber yield to raise the economic value of mangroves and prevent their conversion.

Over-exploitation: The other major interior threat to Asian mangroves is over-exploitation for charcoal, fuelwood, timber (FAO, 2007).

Bangladesh and India (in the Sundarbans), but also Malaysia (e.g. the Matang Mangrove Forest Reserve) and Indonesia have a long-standing tradition in the commercial exploitation of mangroves
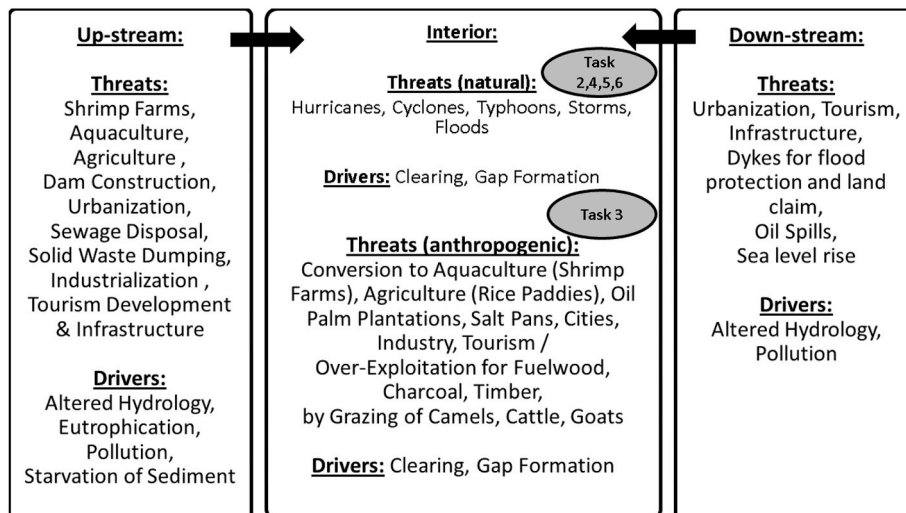
Fig. 1. Interior (anthropogenic & natural), up- and down-stream threats to mangroves and their drivers.

(Faridah-Hanum et al., 2014; Goessens et al., 2014). According to these authors this generally works as follows: Logging companies are given concessions to grow mangroves and harvest the wood of an area. Mangrove forests are grown from natural regeneration on previously clear-cut areas over rotation periods of 20–40 years depending on the species in focus. Natural regeneration is sometimes facilitated by seed trees (as in Indonesia) and sometimes it is assisted by replanting of seedlings/saplings to close rejuvenation gaps. Frequently production forest areas are surrounded by protection zones along the shoreline or along river banks and/or enclosed by buffer zones that provide additional input of propagules. The silvicultural practice of intermediary thinning reduces competition and helps to remove unwanted species. The final harvest is done either as clear felling or as strip-wise felling (Faridah-Hanum et al., 2014; Goessens et al., 2014).

The sustainable mangrove exploitation is a major application domain of IBMs, which operate on small areas of forest stands, such as KiWi and the new IBM mesoFON. Here, the purpose of individual-based models is to evaluate the sustainability of the current management system, to unveil alternative scenarios with maximum sustainable timber yield and to reduce possibly the pressure of over-exploitation to adjacent mangrove areas.

It is likely that subsistence cutting by local communities constitutes also a large portion of mangrove over-exploitation. Furthermore, the harvesting of fuelwood and grazing of camels, cattle and goats are forms of mangrove over-exploitation that are being reported for India, but they also play a crucial role in arid and semi-arid countries of Africa (FAO, 2007). IBMs have not been applied to these forms of over-exploitation. Because of the complexity of involved processes functional-structural models might be more suitable for their simulation. For further anthropogenic threats see chapters 2.3.2 and 2.3.3.

2.3.1.2. Natural threats. Tropical storms and floods are major natural threats to mangroves. On the other hand, a major ecosystem service of intact mangrove forests is the protection of human settlements against the perils of storms/floods (Salem and Mercer, 2012). A key model purpose is, thus, to govern the management of mangrove forest stability for coastal protection. As will be outlined below a combination of mechanistic windthrow models and IBMs is required for this.

So far, the investigation of mangrove responses to natural disturbance represents the second major application area of IBMs, such as KiWi and the new IBM mesoFON, which operate on small areas of forest stands (Piou et al., 2008; Vogt et al., 2014; Grueters et al., 2014). Yet, none of these authors considered that hurricanes do not impact trees by chance (alone). But mechanistic windthrow models do. In mechanistic

windthrow models trees are more likely to break or get uprooted by high wind speeds, if they have larger crowns, thinner and higher stems of lower wood density and are being located in less dense forests, near forest edges or on muddy soil (Gardiner et al., 2000; Peltola et al., 1999).

Presumably, these models could explain what is reported about impacts of tropical storms on mangrove forests by Lugo (2008). In recent years much effort has been made to extend (hybrid–) mechanistic models for uneven-aged, mixed-species forest stands including complex harvesting scenarios and gap formation (WindFIRM/ForestGALES_BC, Byrne, 2011). This effort has opened the way to mangrove forest applications and, in combination with remote-sensing and GIS data, to a model-driven management of mangrove forest stability for coastal protection (compare Mitchell and Ruel, 2015).

A combination of MWMs with IBMs is required, because species have differential reproductive strategies to recover from uprooting or stem breakage. For example, after the passage of hurricane Andrew over South Florida in 1992 "*Avicennia* and *Laguncularia* sprouted vigorously, but *Rhizophora* did not and it regenerated quicker by recruiting seedlings" (Lugo, 2008). Hence, future more realistic mangrove IBMs shall embrace the re-sprouting as well as the localized propagule dispersal mechanism.

2.3.2. Up-stream threats to mangroves

A) Eutrophication: In a fragmented landscape altered land uses cause important up-stream threats to riverine, estuarine and deltaic mangroves that receive water discharge from them. Effluents from (semi-)intensively-managed shrimp farms are known to cause severe nutrient loading and chemical pollution to those mangroves (Robertson and Phillips, 1995; Primavera, 2006). N- and, in particular, P-loading is even higher, when - during shrimp harvest - pond sediment of unused feed is disposed as solid waste in mangrove forests (Robertson and Phillips (1995). By comparison with average N/P-requirements of *Rhizophora*-dominated mangrove forests these authors estimated that for each hectare (ha) of intensive shrimp culture 8 ha of mangrove are required to withdraw the effluent N and 22 ha mangrove are necessary to withdraw the effluent P. As useful as this approach is, it has certain weak points: The estimation is based on average mangrove N/P requirements and on unrealistic assumptions, i.e. (1) tissue N/P concentrations and (2) production rates are independent of the N/P supply by the effluents, (3) effluents are the sole N/P source to the trees (Robertson and Phillips, 1995).

Hence, the main purpose of IBMs regarding eutrophication shall be to provide realistic estimates of the N/P withdrawal capacity of

mangrove forests by accounting for (1) the variation of tissue mineral concentrations and (2) the associated variation in production rates under (3) the influence of elemental cycles including all N/P inputs to as well as all outputs from the mangrove ecosystem.

In the following we will examine, whether mangrove IBMs are ready to achieve this purpose.

Ad 1) On the one hand, this point calls for a mass-balance approach to simulate the uptake of nutrients from the soil. On the other hand, it requires us to include the cycling of nutrients in the IBM, because litter decay replenishes soil nutrient concentrations. So far, only the process-based NUMAN model combined with the IBM FORMAN simulates the decomposition of labile carbon (C) fractions in leaf and fine root litter and refractory C fractions in twig/stem, leaf and fine root litter as well as the remineralization of labile/refractory N/P in these components. However, the model had to lump N/P inputs from dry and wet deposition, N fixation and tidal exchange together, because not enough information about individual processes was available at that time. New models could disentangle these processes as our understanding of elemental cycling under the influence of hydroperiod and soil redox status has strongly improved since then (compare (3) below).

Ad 2) For historical reasons, only the production- and growth-limiting effects of phosphorus have been parameterized and included in mangrove IBMs. In principle, the methodology is extensible to nitrogen on the basis of NH_4^+/NO_3^- measurements in the soil. Once a nitrogen parametrization for IBMs has been accomplished, the question of how to couple the N and P reduction factors needs to be addressed. Since there is mounting evidence of N/P co-limitation from meta-analyses of fertilization experiments (Elser et al., 2007; Harpole et al., 2011) a multiplicative coupling seems appropriate. The whole approach contains two weaknesses. First, it requires laborious measurements of soil nutrient levels as long as their cycling is not simulated in the model. The second weak point is more hidden. In the end, the nutrient concentrations as well as the fitted empirical growth functions depend on all the processes of the respective elemental cycles.

Ad 3) This point has not been addressed in IBMs yet. Important N/P imports other than pond effluents might originate particularly from tidal exchange (Alongi, 2009), from other agricultural land uses (erosion, fertilizer, Kroon et al. (2012) via surface water and possibly groundwater flow (Rasiah et al., 2005 and from rain. Furthermore, the excessive P in effluents from shrimp ponds might fuel N fixation leading to additional N inputs (Rojas et al., 2001; Alongi, 2009).

The consideration of elemental cycles will put further constraints on the respective IBM purpose. The refined purpose shall be to locate mangrove sites along the hydroperiod gradient with high nutrient withdrawal capacity but low risk of nutrient loss due to burial into soil (P) or out-welling into adjacent coastal ecosystems. This can be derived from the following patterns of the regular elemental cycling within mangrove ecotones (graphically summarized in Fig. 2).

Hydroperiod and soil redox potential have a tremendous influence on the unfolding of the elemental cycling. In medium to high intertidal systems burial of available P in sediments (Alongi, 2009; Twilley, 2009), and partial N losses due to anaerobic ammonium oxidation (anammox) and denitrification (Fernandes et al. (2016)) will rather dominate. In low intertidal systems N/P transformation into mangrove biomass (Twilley, 2009), but also a likely surge in the out-welling of particulate and organic N/P into connected coastal ecosystems will prevail. It should be noted here that the soil redox potential and, thus, the elemental cycles are strongly influenced by bio-turbation and burrowing of leaf litter done by the ecological engineers of the mangroves, the sesarmid or ocypodid crabs (Cannicci et al., 2008). Mangrove crabs have been simulated individual-based (Meynecke and Richards, 2014), but not their influence on elemental cycles.

To conclude, in many respects mangrove IBMs are not ready to achieve this purpose. The ecosystem process of elemental cycling needs to be included and the IBMs will have to operate at larger spatial scale.

B) Alteration of the hydrological regime and hydro-

geomorphological changes: A number of up-stream threats, such as agricultural land use, urban and industrial development, adversely affect mangroves by the alteration of the hydrological regime. Freshwater inflow is diverted - sometimes remotely - by the construction of dams for power generation and irrigation of agricultural land and – locally - by drainage for urban settlement or agricultural use (Lacerda, Luiz D. de and Linneweber, 2013; Dahdouh-Guebas et al., 2005). Reduced freshwater inflow may cause the intrusion of seawater thereby endangering less salt-tolerant mangrove species, such as *Heritiera fomes* Buch.-Ham. in the Sundarbans (resulting from the Farakka Barrage, Sarker et al., 2016). The concomitant reduced groundwater flow might retain more salt in the sediment which is left behind there by salt-excluding mangrove species (Wolanski and Elliott, 2015). Moreover, dams trap large volumes of coarse sediment, thereby starving estuarine mangroves of sediment (Wolanski and Elliott, 2015). The impact of these hydro-geomorphological changes, such as coastal erosion, coastal recession and sinking deltas, might take decades to become apparent, but will be probably the most permanent ones (Wolanski and Elliott, 2015).

Hydraulic models have been used to simulate the balance of freshwater and saltwater inflows in response to coastal engineering projects (Marois and Mitsch, 2017; Di Nitto et al., 2013), but certain ecosystem models have similar capabilities (compare ch. 4.1). The purpose of IBMs in combination with hydraulic models shall be to predict the implications of an altered hydrology, salinity and sedimentation for mangrove communities. Because hydrological changes also abound among downstream threats, we postpone the discussion whether IBMs are ready to achieve this purpose to the next chapter.

2.3.3. Down-stream threats to mangroves: deprivation of the regular tidal cycle

All down-stream threats are anthropogenic, e.g. urbanization, industrialization including port construction, and tourism development. They deprive mangroves of the regular tidal cycle by way of dykes for flood protection and land claim, by roads and by other infrastructure (Wolanski and Elliott, 2015). The hydroperiod has been proposed as a key factor controlling the zonation of mangrove species as early as 90 years ago (Watson, 1928; as quoted by Crase et al., 2013). Hence, the implications of such altered hydrological signature for mangrove communities are likely substantial. Determining the normal hydrology (depth, duration and frequency of tidal flooding) in existing natural mangrove communities, as reference sites, is also the most important factor in mangrove restoration (Lewis, 2005). So far, the interaction of the hydroperiod with other site conditions, such as resource and regulator gradients, lacks clear scientific understanding (Twilley and Rivera-Monroy, 2005; Krauss et al., 2008).

IBMs have not made much progress towards a mechanistic simulation of those interactions in recent years. Twilley and Chen (1998) presented the hydrological model HYMAN, which is combined with the IBM FORMAN and simulates the daily water table and salinity as the combined effect of tidal exchange, rainfall, runoff, seepage and evapotranspiration. While their work is particularly valuable for the measurement and calculation of the Rockery Bay water budget, the HYMAN model, as pointed out by Twilley and Chen (1998) has a number of limitations. First and foremost, it lacks a true coupling with the vegetation because it administers merely potential evapotranspiration via the Penman equation (Penman, 1948). Commonly such coupling is achieved by extending the standard Penman-Monteith equation by the mean stomatal conductance of the leaf area index and the boundary layer conductance (Jones, 2014). The following example illustrates how important the application of such an approach is: Barr et al. (2014) found a subtropical mangrove forest to behave like a semi-arid ecosystem during the dry season with high salinity levels resulting in reduced canopy conductance and causing evapotranspiration to decline.

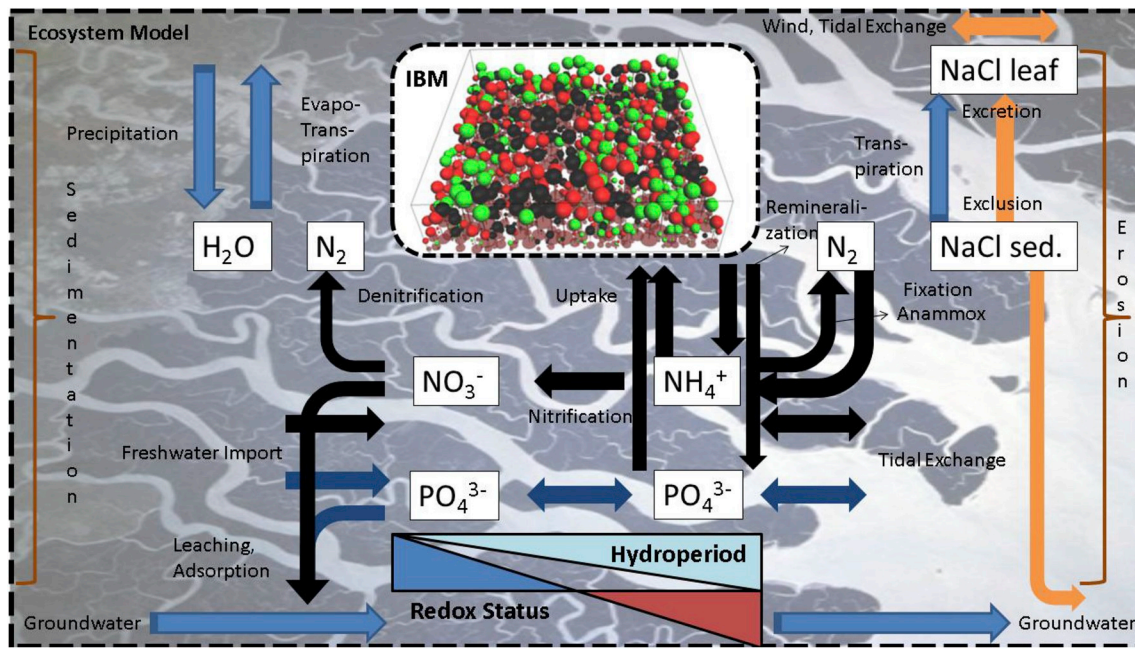Mechanisms considered to be responsible for the hydroperiod-

Fig. 2. Sedimentation/erosion & water, salt, nitrogen, phosphorus cycling in mangroves along gradients of hydroperiod and redox status. For further explanation of the involved processes see ch. 2.3.2, ch. 2.3.3.

related mangrove zonation are: species-specific differences in (1) tree traits related to water use (Ball and Passioura, 1994) and (2) in the competitive responses to salinity and resources, (3) propagule sorting by tides (Rabinowitz, 1978; Clarke et al., 2001) and (4) selective predation of propagules by crabs (Dahdouh-Guebas et al., 1998, 2011; Krauss et al., 2008; Crase et al., 2013). We expect it to cover points (1,2,3) if an individual-based mangrove stand model (KiWi or the new IBM mesoFON) is integrated in an ecosystem model. In case we are not able to resemble observed species zonation patterns by this integrated model, the next step should be to append the simulation of propagule predation by crabs (point (4)) following the conceptual framework of Cannicci et al. (2008).

This proposed mechanistic perspective as a whole will increase in relevance in the future, when the mangrove ecotone starts to move at large in response to sea level rise (Krauss et al., 2014).

3. The recent development of mesoFON

3.1. The initial development

mesoFON is a new individual-based model of mangrove forest dynamics that was developed from the KiWi model and first described by Grueters et al. (2014). The authors provided a full model description according to the ODD (overview, design concepts, details) protocol (Grimm et al., 2006, 2010).

mesoFON advanced beyond current mangrove IBMs by describing crown plasticity of mangrove trees. This was motivated by the finding that the approximation of crowns as rigid cylinders in the SORTIE forest growth model led to unrealistic behavior, such as stronger crown overlapping and more gap formation (Pacala and Deutschman, 1995). As this was identified to be the most critical biological shortcoming of the SORTIE model (Pacala et al., 1996) its developers made considerable effort to enable simulated crowns to move laterally and to change their shape flexibly or, in other words, to make them plastic (Strigul et al., 2008).

Grueters et al. (2014) presented results of a first mesoFON application. They examined the long-term interaction of lateral crown displacement and disturbance in mangroves and addressed tasks 2, 5 and 6 thereby (see Table 1). The purpose of the first mesoFON model was thus

purely task-oriented.

The crown plasticity routines in mesoFON take advantage of the fields-of-neighborhood (FON) approach originally proposed by Berger and Hildenbrandt (2000). Grueters et al. (2014) duplicated the FON of a tree, one being responsible for above-, the other being responsible for belowground competition. They shift the above-ground FON and the crown (center) together away from the most severe competition in its neighborhood, thereby allowing for lateral crown displacement and competitor avoidance.

Grueters et al. (2014) conducted simulation experiments with two plant functional types (PFTs) of the red mangrove (*Rhizophora mangle*). While one functional type possessed plastic crowns, the other PFT had rigid crowns. They exposed them either in monoculture or as a community, to two disturbance regimes, namely (1) without disturbances and (2) with hurricane impacts returning every 5 years.

The main results from the first mesoFON application were as follows (compare Table 2): without disturbance crown movements increased only the stand-based stem volume, because high competitive strength constrained the effects of plasticity in dense undisturbed stands. Yet, in disturbed stands, the plastic behavior of the crowns strongly raised stem volume as well as tree density as a result of substantially reduced local competition. Here, crown shifts were particularly advantageous because of their contribution to gap closure.

A major difference of mesoFON, at least in comparison with the KiWi model, is the way it simulates tree recruitment. The default KiWi version had remained in the stage of the JABOWA type model and added constant numbers of saplings for each species each year. It simulated mangrove community dynamics like "trapeze acrobatics with a safety net", because a worse competitor could never get extinct. Conversely, in mesoFON propagule production was made individual-based (Grueters et al. (2014). Larger parental trees and those growing under better conditions produce more offspring by assuming a constant optimal propagule density per crown surface area which is downregulated by local competitive/environmental constraints. Offspring was still placed randomly on the plot in the first application, while the second reached the stage of the SORTIE model by introducing localized propagule dispersal around parental trees via a negative exponential dispersal kernel (Grueters et al., in prep.). The tree life cycle was closed by this and from this moment mesoFON can be considered as a true IBM.

Table 2
Main results of the interaction of crown plasticity and disturbance regime in the first mesoFON application (Grueters et al., 2014) including results of t-tests PFT_rigid =
   plant functional type with rigid crowns, PFT_plastic =
   plant functional type with plastic crowns.

Treatment	Variable	PFT_rigid			PFT_plastic			Change		Change
		Mean	SD	SE	Mean	SD	SE	p-value, sign.	± %	± %
Without Disturbance	stem volume [m³ ha⁻¹]	621.86	14.22	0.30	663.42	14.34	0.22	0.0001 ***	6.68	
	density [ha⁻¹]	843.89	12.71	0.21	847.45	14.18	0.15	0.0033 **	0.42	
	competition (x 10⁶)	193.29	7.18	0.18	189.59	7.67	0.13	0.0023 **	-1.92	
With Disturbance	stem volume [m³ ha⁻¹]	333.01	17.29	0.69	374.72	18.44	0.49	0.0003 ***	12.52	
	density [ha⁻¹]	746.24	26.16	0.83	801.87	27.85	0.59	0.0002***	7.45	
	competition (x 10⁶)	122.90	8.19	0.40	98.16	6.18	0.28	0.0003 ***	-20.14	

3.2. The model calibration for Rhizophora apiculata

Based on arguments given in chapter 2.2 we identified an urgent need to parametrize individual-based mangrove forest models for Asian tree species in particular. In this chapter, we present a mesoFON calibration for the economically important Asian mangrove species *Rhizophora apiculata*. In this study we retrieve the best parameter set by way of Genetic Algorithms (GA). GA are a heuristic global optimization technique mimicking the action of natural selection, crossover and mutation to solve (such) hard optimization problems (Hamblin and Hansen, 2013). Because soil nutrient levels were not available yet, we used inverse modeling techniques to infer them. Hence, the retrieved parameters have to be considered as preliminary.

The study is based on data of tree positions, stem heights and stem diameters at 1.37 m height. The data was collected in the Matang Mangrove Forest Reserve in the West of peninsular Malaysia on 36 plots of 10 m × 10 m, at an age of 7, 15, 20 and 30 years.

3.2.1. Forest management in the Matang Mangrove Forest Reserve

The Matang Mangrove Forest Reserve has been used for the production of charcoal and construction wood since 1902 and is therefore one of the oldest commercially exploited mangrove forests worldwide. *Rhizophora apiculata* trees are grown over rotation periods of 30 years in the reserve. The trees develop by natural regeneration from propagules that are produced by mature trees of the previous generation and survive the clear cutting on the plots (in part protected by the aerial root network which is not cut in the Matang area). The production forest areas are surrounded by protection zones along the shoreline or along river banks and/or are enclosed by buffer zones, all of which provide additional input of propagules. Natural regeneration is assisted by re-planting of seedlings/saplings in the second year if necessary, but the trees also commence generative reproduction at an early age of a few years and contribute to propagule input thereafter. The silvicultural practice on concessional areas consists of two intermediary thinning events which remove competing dominant trees at a distance of 1.2 m from pre-dominant trees in year 15 and at a distance of 1.8 m in year 19. The final harvest is done as clear felling in year 30.

3.2.2. Explorative data inspection

Maximum tree size is considered to be least influenced by management (Pretzsch, 2009) and therefore maximum tree size is used in this section as a proxy for the tree response to competition and environment. Maximum tree sizes of *Rhizophora apiculata* in the 7- year-old plots varied little and ranged from 12.4 m height and $d_{1.37}$ of 9.2 cm to 12.6 m height at $d_{1.37}$ of 8.7 cm.

In the four 15-year-old plots the maximum *R. apiculata* size remained at best at a height of 12.6 m and a $d_{1.37}$ of 10.1 cm – indicating worse environmental conditions in those plots compared to the 7-year-old plots. Soil samples were taken for the analysis of NH_4^+, NO_3^- and PO_4^{3-} concentrations on all plots and salinity was examined selectively

on the four 7- and the four 15-year-old plots at a single time. Measured salinities amounted to between 18 and 20 parts per thousand (ppt). As these values lie well in the reported range of vigorous *R. apiculata* growth (Barik et al., 2018) we ruled out salinity as growth-limiting factor (but see ch. 3.2.4 for the details of this decision). On the basis of general conclusions on tropical mangroves (Reef et al., 2010; Hossain and Nuruddin, 2016) and reported leaf N:P-ratios (Lovelock et al., 2007) we assume here that phosphate is the sole growth-limiting nutrient (but see ch. 3.2.4 for the details of this decision) and suppose further that *R. apiculata* and *R. mangle* respond identically to phosphate.

Variation of maximum *Rhizophora apiculata* tree sizes was much higher among 20- and 30-year-old plots. In 20 year-old plots maximum height/$d_{1.37}$ could be as high as 39.2 m/34.2 cm and as low as 16.5 m/14.4 cm. Tree densities were similar among those plots (in contrast to plot 8 below), but plots with a smaller maximum tree size seemed to be relatively thicker (i.e. had a smaller height-diameter ratio) than those with a taller one (data not shown). In accordance with our previous work (compare Vovides et al., 2014) this suggests, that soil nutrients were responsible for the slower growth and for the smaller height-diameter ratio in the former plots.

The largest stand-based stem volume was obtained on a 30-year-old plot (plot 0) inhabited by only three large *Rhizophora* trees and maximum tree size of 40.0 m/44.2 cm. It amounted to 9.15 m³ (or 915.22 m³/ha).

Conversely, in another 30-year-old plot (plot 8) inhabited by 26 *Rhizophora apiculata* trees the maximum tree size amounted to 42.0 m/37.5 cm. Therefore, trees under strong (above-ground) competition tended to exhibit larger height-diameter ratios and invested more in height growth to escape shading (Vincent and Harja, 2007). Despite the high tree density, the attained stand-based stem volume on this plot was only at 5.12 m³ (512.41 m³/ha).

Trees belonging to other species were also present on the plots, even though less in number and size. Among the 479 trees on 20- and 30-year-old plots 295 belonged to *R. apiculata* (61.6%) 130 to *Bruguiera gymnorhiza* (L.) Savigny (27.1%), 30 to *Bruguiera cylindrica* (Linnaeus) Blume (6.3%), 14 to *Bruguiera parviflora* (Roxb.) Wight & Arn. ex Griff. (2.9%), 5 to *Bruguiera sexangula* (Lour.) Poir. (1.0%), 4 to *Rhizophora mucronata* Lam. (0.8%) and 1 to *Ceriops tagal* (Pers.) C.B.Rob. (0.2%). In younger plots only 3 *Rhizophora mucronata* were among a total of 1361 trees; the remaining trees on those plots belonged to *R. apiculata*. The pioneering species *Avicennia alba* Blume commonly found on newly-formed mud banks in the area was not present on the plots due to their somewhat more landward location.

3.2.3. GA optimization strategy

From the above described forest management scheme with its continual input of propagules over the entire rotation period it is evident: It was not appropriate to perform the model initialization - as usual - with a number of randomly distributed saplings and grow them to the plot age in the simulation.

Instead we used mesoFON here as a "way-back machine", initialized the model with the individual trees sized at observed stem diameters (i.e. $d_{1.37}$) and located at observed positions, ran the time backwards and shrank the trees to sapling size until the plot age of 1 year. The mean squared deviation between tree heights observed on the plots and initial tree heights simulated via eq. (7) was used as the fitness criterion to be minimized in the GA. As detailed in chapter 3.2.4 the initial height of a focal tree was determined assuming a constant (height [cm] – 137)/diameter [cm] ratio in the absence of other influencing factors and was otherwise refined on the basis of the tree's above- and/or below-ground competition including the soil phosphorus content. By this means, a pattern-oriented modeling strategy (Grimm and Railsback, 2005) was put in effect. In principle, the fitness criterion is calculated for the entirety of individual trees on all plots to cover the large inherent variation of ontogenetic stages, competitive settings and environmental conditions among plots (see ch. 3.2.2 above). Moreover, "wrong behavior" is punished by adding penalties to the fitness (constrained GA, Yeniay, 2005). We consider as wrong behavior: (1) that all trees have shrunken to sapling size before the plot age of 2 years is reached, (2) that trees have "died" from competition before they have shrunken to sapling size, (3) that trees were felled at plot age 15 or 19 years or (4) that trees have remained alive and well as a tree on the site at a plot age of 1 year. Additionally, we used a repair algorithm (Yeniay, 2005) to choose soil phosphorus contents (which we assumed were solely responsible for the variation in tree growth among plots, compare ch. 3.2.2) that led to correct shrinking (growing) behavior. This is done with a bisection solver which finds the root (P level) of a discontinuous function that returns -1 when trees are too slow, 1 when trees are too fast and 0 when the shrinking speed is just right. In essence, it is this repair algorithm that transforms the seemingly superficial fitness criterion referred to above (i.e. the mean squared deviation between tree heights observed on the plots and tree heights simulated by the model at initialization) into a fitness criterion that is highly robust and covers all tree growth processes simultaneously. Primarily, the slowest shrinking/growing trees, those being tallest or those being exposed to the most severe competition, govern the repairing and ultimately the growth processes.

Let us illustrate the procedure with the following simplified example of an individual tree that is present on a 7-year-old plot with optimum P content and has no competing trees in its neighborhood: The stem diameter $d_{1.37}$ measured on the tree at the plot age of 7 years amounted to 11.24 cm and its measured height was 1200 cm or 12.00 m. If the growth-related parameters, part of the so-called genes of the GA, in this run were the maximum diameter growth rate of a sapling $\Delta d_{max} = 1.8$ cm yr^{-1}, the maximum stem diameter at 1.37 m height $d_{max} = 50$ cm and the maximum stem height $h_{max} = 5000$ cm (compare eq. (6)) the model would calculate the current height of the tree via the height function of eq. (7) to be at $((h_{max} - 137)/d_{max}) \times d + 137 = 1230$ cm $= 12.30$ m. In the absence of competition, the model would compute the following series of

diameters [cm]	11.24	7.96	4.84	2.21	0.66	0.15	0.03	and
heights [m]:	12.30	9,11	6.08	3.52	2.01	1.51	1.40	in
simulated year	0	1	2	3	4	5	6	at
plot age [yrs]:	7	6	5	4	3	2	1	

Therefore, the tree had reached the threshold to the sapling stage (d = 0.03 cm, assumed) at the plot age of year 1. It did neither shrink too slow nor too fast. Hence, no penalty was triggered and no repairing was necessary. In that case, the deviation would amount to $(12.30–12.00) = 0.30$ m or 0.09 m^2 squared.

The GA optimization routines were coded with the Java Genetic Algorithm Package (JGAP, Meiffert, (c) 2000–2018) and were made an integral part of the mesoFON model to achieve flexibility. We ran the GA over 50 generations with a population of 50 chromosomes (= model parameter sets), each on all 36 plots. In accordance with recommendations for JGAP the crossover rate was set to $0.35 \times$ population size $\times$ optimized genes/(all genes in a chromosome) and the mutation rate was set to 1/(length of optimized genes in a chromosome). We allowed for the initial injection of a penalty-free and supposed to be best chromosome. We iterated the run with the previous best solution being reinjected.

The GA optimizer was utilized as a guiding tool for further model refinement by watching data points of the trees and their linear regression move in a "simulated height" vs. "observed height" plot. Whenever a strong systematic deviation from the 1:1-line was observed, something was "in the way" of the optimizer and suitable adjustments were made by us. This optimizer-driven development of ecological models (ODEM) led to fundamental model alterations described below.

3.2.4. Model description according to the ODD protocol

In accordance with chapter 2.3.1 the mesoFON purpose was redefined for this application: By now, the model purpose is to evaluate the sustainability of the current management system and to unveil alternative scenarios with maximum sustainable timber yield.

State variables of an individual tree in this IBM are: stem x,y-position, (shifted x,y-position of the crown center, turned off due to lack of data), stem height, stem diameter at 1.37 m height ($d_{1.37}$), age and the average stem volume growth of a preceding time period. A central, derived variable is stem volume assuming a form factor of 0.65 for *R. apiculata*.

Scales: The spatial scale is 10 m $\times$ 10 m during the calibration. The plot is surrounded by an empty margin of 10 m. This prevents marginal trees to affect each other across periodic boundaries. All trees on the plot grow, but only those in the central 8.5 m $\times$ 8.5 m area of the plot contribute to the fitness calculation. By this means, we reduce artifacts resulting from the empty margin. The spatial scale will amount to several hectares later on. In the calibration the model is run in annual time steps for 30 years at maximum. This will increase later as some protected areas in the Matang Mangrove Forest Reserve are more than 90 years old.

Process overview and scheduling: The processes accounted for in this model are scheduled in the following order: (1) tree recruitment including propagule production and dispersal (both turned off in early calibration), (2) above-ground competition implicitly for light and below-ground competition influenced by salinity and soil phosphorus content, (3) stem volume growth, (4) tree mortality (turned off during early calibration), crown plasticity (turned off due to a lack of data), forest thinning (turned off in early calibration). The processes contained in mesoFON are graphically illustrated in Fig. 3 and a brief verbal description of the mesoFON design and structure is given in Table 3.

Resource description: In principle, mesoFON allows for heterogeneous and dynamic resources (P content) and regulators (salinity) via the import of grey-scale images, but during the calibration we assume a homogeneous and static distribution within a plot.

Design concepts: The focus lies on the simulation of stem volume growth. The (final) height-diameter ratio (h-d ratio) is dynamically shifted according to the severity of above-vs. belowground constraints. Stem volume growth rate is reduced by above-/below-ground competition (simulated via Fields-of-Neighborhood, FONs) as well as by salinity and soil phosphorus content.

Emergence: The macro-scale behavior of the stand emerges from the micro-scale processes at the level of individual trees.

Sensing and interaction: An established tall-stilt mangrove tree senses the influence and identity/position of competitors inside its above- and below-ground FON surrounding and thereby interacts with its neighbors. Below-ground, it probes the environment at the position of its trunk origin and acts accordingly.

Stochasticity: There are no stochastic processes included during calibration. Initial locations of tree saplings are chosen at random when time is run forward in later simulations.
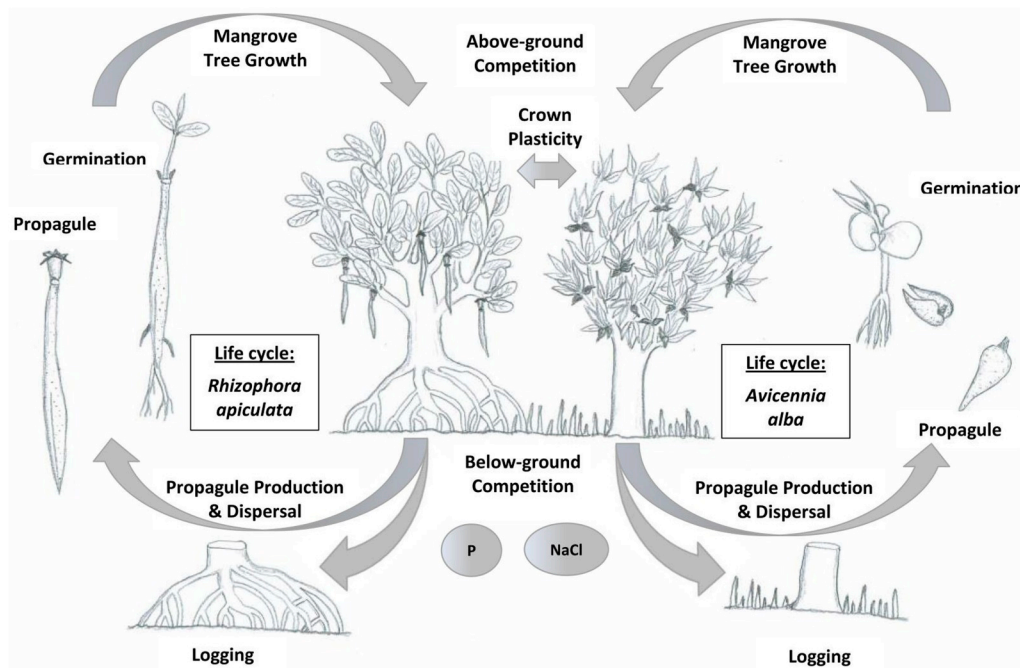
Fig. 3. Mangrove life cycles and processes contained in mesoFON, exemplified with the interaction of the Asian (Malaysian) mangrove species *Rhizophora apiculata* Bl. and *Avicennia alba* Bl.

Observation: During optimization mesoFON provides a chart of fitness values (best fitness, mean fitness ± std. dev., worst fitness) vs. GA generations and print-outs of further optimization diagnostics.

Initialization and input: The model is initialized with trees sized at observed stem diameters ($d_{1.37}$) and located at observed positions for the calibration. Later, the model will be initialized with randomly and uniformly located tree saplings.

3.2.4.1. Sub-models. Competition among trees: Competition is simulated via a duplicated "Field-of-Neighborhood" FON approach, one being responsible for above-ground competition, one being responsible for below-ground competition. The following equations describe the approach (Berger and Hildenbrandt (2000).

At radius r [m] the intensity of above-ground competition exerted by a tree is given by

$$
FON(r) = \begin{cases}
for\ 0 < r \le r_{1.37} & \rightarrow I_{max} \\
for\ r_{1.37} < r \le R_{FON} \rightarrow \frac{I_{max}}{e^{c \cdot rbh}} \cdot e^{c \cdot r}, \\
c = \ln(I_{min})/\ (R_{FON} - r_{1.37}) \\
for\ r > R_{FON} & \rightarrow 0
\end{cases}
\tag{1}
$$

where $r_{1.37}$ is the radius of the trunk at 1.37 m height [m].

Table 3
Structure and design of mesoFON. The layout of this table is identical with that of Table 1 in Berger et al. (2008) to ease comparison with FORMAN, KiWi and MANGRO.

Model purpose	to evaluate the sustainability of the current management system and to unveil alternative scenarios with maximum sustainable timber yield
State variables	stem x,y-position, stem height, stem diameter (d1.37). stem volume (derived), age, average stem volume growth over a preceding time period, (shifted x,y-position of the crown center, turned off due to lack of data)
Processes	Tree recruitment: propagule production & dispersal (turned off in calibration) competition, above-ground for light (implicitly) competition below-ground, influenced by salinity, P content stem volume growth mortality & tree thinning (turned off in early calibration), crown plasticity (turned off, due to a lack of data)
Spatial scale	several hectares, 10 m × 10 m (calibration)
Resource description	heterogeneous & dynamic, homogeneous (calibration)
Design concepts	Focus is on stem volume growth with dynamic height-diameter ratio, growth rate reduced by above-/below-ground competition, salinity, P content Emergence: stand behavior emerges from behavior of individual trees Sensing and interaction: a tree senses influence of competitors inside its above-/below-ground FON, it interacts with neighbors thereby. Below-ground, it probes the environment at the stem position and acts accordingly.
Initialization	randomly placed saplings, trees sized at observed d1.37 & observed positions (calibration)
Sub-models	see chapter 3.2.4

R_{FON} is the radius [m] of the FON

I_{max} is the maximum intensity of above-ground competition (inside the trunk)

I_{min} is the minimum intensity of above-ground competition at R_{FON}, defined as a fraction of I_{max}

The structure of eq. (1) ensures that the FON intensity declines exponentially from I_{max} at the trunk to I_{min} at the FON margin. The equation used for below-ground competition is identical, except that $I_{max, below}$ replaces I_{max} and $I_{min, below}$ replaces I_{min}. Grueters et al. (2014) set $I_{min, below}$ to 0.999 to ensure size-symmetric below-ground competition (Casper and Jackson, 1997).

The increase in the FON radius [m] with increasing tree size is governed by the following allometric relationship:

$$R_{FON} = a \cdot (r_{1.37})^b \tag{2}$$

where a is the allometric coefficient and b is the allometric exponent.

The local intensity of above-ground/below-ground competition at an x,y-location in the plot area is given by eq. (3). In principle it is obtained by adding the intensities of all n above-ground/below-ground FONs that have non-zero intensity at x,y and overlap with the co-ordinate.

$$F(x, y) = \sum_n FON_n(x, y) \tag{3}$$

The above-ground/below-ground competitive influence F_A^k of n neighboring trees (n ≠ k) on a focal tree k is then calculated by summing the area-based integrals of all n above-ground/below-ground FON overlaps and dividing each by the sum of the above-ground and the below-ground integral of the focal FON to normalize it:

$$F_A^k = \sum_{n \neq k} F_{A_k}^n = \sum_{n \neq k} \frac{\int_{A_k} FON_n(x, y)da}{\int_{A_k} FON_{k,above}(x, y)da + \int_{A_k} FON_{k,below}(x, y)da} \tag{4}$$

where A_k is the above-ground/below-ground FON area of the focal tree and da is the area variable over which we are integrating.

F_A^k is scaled to a range of [0,1] in case the value calculated by eq. (4) falls outside this range. The generalized normalization step described above is applicable to any I_{max} and I_{min} parameter values.

We make two notable advancements to this set of equations: (1) we take into account the larger radius of the rooting system when compared with the crown radius (below-ground/above-ground FON radius). The respective parameter, the belowground-aboveground ratio (ratio$_{BA}$) being multiplied with eq. (2), is given free to the optimization.

(2) We further give $I_{min, below}$, the minimum below-ground competition at the FON margin, free to optimization thereby allowing for size-asymmetric below-ground competition (in contrast to Casper and Jackson, 1997). This decision was motivated by results of root system studies on *Rhizophora mangle* trees in which root density declined rapidly with increasing distance from the trunk (Berger and Wagner, unpublished).

In total, this sub-model adds 7 parameters to the optimization: a, b, I_{max}, $I_{max, below}$, I_{min}, $I_{min, below}$, ratio$_{BA}$.

Optimal tree growth: When the first 7-/15-year-old plots were simulated, a strong systematic under-estimation of tree heights was detected, indicating that – in contrast to the general assumption of the Shugart growth function (Botkin et al., 1972; Shugart, 1984) – the height-diameter relationship was not quadratic for *R. apiculata*. In the testing of various alternative height-functions (linear, logarithmic, power) the linear function turned out to be most suitable. This means the height-diameter ratio or more specifically (h – 137)/d is independent of a tree's ontogenetic stage. However, the opposite effects of above-vs. below-ground constraints on the h-d-ratio (compare ch. 3.2.2) was employed as follows:

$$corr_{above} = (1 - comp_{above})$$
$$corr_{below} = (1 - comp_{below}) \cdot f_{red, sal} \cdot f_{red, P}$$

$$if \ (corr_{above} < corr_{below})$$
$$\begin{cases} d_{max,dyn} = d_{max} - red_{dmax, above} \cdot (1 - corr_{above}) \cdot d_{max} \\ h_{max,dyn} = h_{max} - red_{hmax, above} \cdot (1 - corr_{above}) \cdot h_{max} \end{cases}$$

$$corr_{below} \geq corr_{above}$$
$$\begin{cases} d_{max, dyn} = d_{max} - red_{dmax, below} \cdot (1 - corr_{below}) \cdot d_{max} \\ h_{max, dyn} = h_{max} - red_{hmax, below} \cdot (1 - corr_{abelow}) \cdot h_{max} \end{cases}$$

$$\tag{5}$$

where corr$_{above}$ denotes the growth correction due to above-ground competition (comp$_{above}$).

corr$_{below}$ is the growth correction due to below-ground competition (comp$_{below}$),

the growth reduction due to salinity (f$_{red, sal}$) and due to soil P content (f$_{red, P}$)

red$_{dmax, above}$ and red$_{hmax, above}$ are two parameters in the range [-1, 1] that reduce or raise d_{max} and h_{max}, respectively, when above-ground competition is more severe (case 1).

red$_{dmax, below}$ and red$_{hmax, below}$ are two parameters in the range [-1, 1] that reduce or raise d_{max} and h_{max}, respectively, when below-ground constraints are more severe (case 2).

The resulting $d_{max,dyn}$ and $h_{max,dyn}$ are then dynamic.

All four parameters are given free to GA optimization. A robust priority allocation algorithm (Ventana Systems Inc., (c) 2015) is set on top of these calculations to make the transition between effects of above- and below-ground competition possibly more smooth. This happens when a larger value for the regulating parameter (width) is chosen by the GA.

Finally, the following function defines the optimum annual increment of the diameter at 1.37 m height Δd/Δt for *Rhizophora apiculata*:

$$\frac{\Delta d}{\Delta t} = \left[\frac{G \cdot d \cdot \left(1 - \frac{d \cdot h}{d_{max,dyn} \cdot h_{max,dyn}} \right)}{234 + 3 b_2 d} \right]$$

$$with \ h = 137 + b_2 \cdot d, \quad G = \frac{(\Delta d)_{max} \cdot h_{max,dyn}}{0.2 \cdot d_{max,dyn}}, \quad b_2 = \frac{(h_{max,dyn} - 137)}{d_{max,dyn}} \tag{6}$$

where d is the diameter at 1.37 m height ($d_{1.37}$) of a focal tree, $d_{max,dyn}$ is the dynamic maximum attainable $d_{1.37}$ in [cm], h is the tree height [cm], $h_{max,dyn}$ is the dynamic maximum achievable height [cm], G and b_2 are two auxiliary variables that link diameter and height growth, $(\Delta d)_{max}$ denotes the maximum initial $d_{1.37}$ growth rate of a sapling and is the third parameter of this function.

The underlying dependency of stem height h on $d_{1.37}$ is thus:

$$h = 137 + b_2 \cdot d \tag{7}$$

This leaves us with 8 parameters to be optimized for this sub-model: Δd$_{max}$, d$_{max}$, h$_{max}$ (all three derived from plot 0, assuming P = 369.46 g/m²), red$_{dmax, above}$, red$_{dmax, below}$, red$_{hmax, above}$, red$_{hmax, below}$, width.

Growth reduction by salinity f$_{red,sal}$: On the basis of the following argumentation we derive that growth reduction by salinity is negligible on our plots.

Information on the salt tolerance of *Rhizophora apiculata* or its fundamental niche in terms of salinity is only available from experiments in which seedlings were grown over a limited time period at a range of salinities (Moorthy and Kathiresan, 1995; Ball et al., 1997; Basyuni et al., 2018, 2019; Kodikara et al., 2018). However, the results of these experiments vary considerably in detail. Basyuni et al. (2019) report maximum seedling dry weight in their freshwater treatment.

Moorthy and Kathiresan (1995) found a peak seedling biomass at a salinity of 5 parts per thousand (ppt) (in the NH_4^+ treatment) with a sharp decline below and above a narrow range of 5–10 ppt. Ball et al. (1997) report a 40% decrease in the seedlings' relative growth rate (RGR) between 9 and 27 ppt in the ambient CO_2 × humid air treatment and an even more severe RGR drop in the corresponding dry air treatment. Basyuni et al. (2018) found an optimum seedling dry weight at 15 ppt and a more bell-shaped salt tolerance curve. In the longer-term study conducted by Kodikara et al. (2018) the low salinity treatment (3–5 ppt) provided the best conditions for seedling growth of *R. apiculata* and 5 other mangrove species until 15–20 weeks of age, but afterwards the optimum salinity shifted towards 15–17 ppt. Such plasticity of salinity tolerance during ontogeny has been described repeatedly for mangrove species (Kathiresan and Bingham, 2001; Alleman and Hester, 2011). With 18–20 ppt the salinity measured on our plots was close to the optimum reported by Kodikara et al. (2018), but the trees varied in age with the oldest being 7 or 15 years of age on respective plots. Because the progression of salinity tolerance with age is rather unknown, we decided to rely our assessment of salinity effects additionally on the realized niche which is commonly believed to be a subset of the fundamental niche (Chase and Leibold, 2003). Based on its distribution in the Sundarbans *Rhizophora apiculata* is considered to be an indicator species for mesohaline conditions and is abundant only in the salinity range between 15.1 and 25 ppt (Barik et al., 2018).

As salinities measured in this study fell well in this range, we assumed negligible growth reduction due to salinity and set $f_{red, \; sal}$ accordingly to 1 on all plots. Further salinity measurements are likely required to cover the prevailing spatiotemporal heterogeneity in salinities (Robert et al., 2009), to derive a salinity tolerance curve for *R. apiculata* and to finally verify our decision.

Growth reduction by phosphorus content: Mangroves of the tropics are expected to be limited by nutrients due to the strong weathering of the old highly leached soils and by phosphorus, in particular, because P - in contrast to N - is not replaced by biological fixation (Reef et al., 2010). A P-limitation to mangrove growth in Malaysia has been inferred by analyses of N:P ratios in leaf tissue (Lovelock et al., 2007; Reef et al., 2010). Moreover, there exists commonly a strong correlation between total (Kjeldahl) nitrogen and phosphorus content in tropical mangrove soils (Table 3 in Hossain and Nuruddin, 2016). Our decision to assume here a sole growth limitation by phosphorus is supported by these arguments. But N has been most frequently observed to limit growth in mesotidal settings of the Indo-Pacific region (Reef et al., 2010) and - as outlined in chapter 2.3.2 – there is mounting evidence of N/P co-limitation of primary producer communities worldwide (Elser et al., 2007; Harpole et al., 2011). Therefore, we consider our decision to be preliminary and a revaluation based on our soil N/P measurements will be necessary in the future.

The growth-reducing effect of phosphorus is given in mesoFON by a quadratic equation that is dependent on the "relative nutrient availability" (RNA, Chen and Twilley, 1998):

$$f_{red, \; P} = c_1 + c_2 \cdot RNA + c_3 \cdot RNA^2 \tag{8}$$

RNA resembles the relative production rate of mangrove forests calculated by using a Monod function that depends on the soil phosphorus content in g/m^2 ground area to a depth of 40 cm (see Chen and Twilley, 1998). Parameters given for *Rhizophora mangle* were retained for *R. apiculata,* but in a corrected form that ensured maximum $f_{red, \; P} = 1$ at RNA_{max} and $P_{max} = 369.46 \; g/m^2$. The three parameters were determined to be: $c_1 = 0.0$, $c_2 = 2.1654$ and $c_3 = -1.17254$ and were held constant during this calibration. Additionally, the arbitrary assumption was made that the P content on the plot with maximum stand-based stem volume amounted to a P level of $369.46 \; g/m^2$ which

maximizes growth.

Tree recruitment: For the number of offspring N (an integer number) being produced by an individual tree per year the following equation is applied:

$$N = f_{red, \; P} \cdot f_{red, \; sal} \cdot D \cdot A \tag{9}$$

where $f_{red, \; P}$ and $f_{red, \; sal}$ are reduction factors assumed to be identical with the growth reduction factors referred to above and D is the species-specific offspring density per crown surface area A in $[m^2]$ assumed to be constant over the lifetime of a tree (1 parameter). Offspring production is turned off at first in the calibration. But once an optimum parameter set is found, the offspring density per crown surface area (parameter D) could be derived from the series of annual sapling disappearance rates observed during backward simulation. The interpretation of these figures is based on the survey of *R. apiculata* seedling development in the Matang mangrove forest reserve carried out by Srivastava and Khamis (1978). The authors report that the *Rhizophora* seedlings/saplings were distributed uniformly and that 10.3% of them had already reached a height of 1.52–3.05 m 12 months after clear-felling. This percentage increased to 53% 12 months later. From these figures we infer: Natural regeneration of *Rhizophora apiculata* plantations in the Matang area starts primarily from propagules that are produced by trees of the previous generation and survive the clear cutting as a seedling/sapling bank on the plots (in part protected by the aerial root network which is not cut in the Ma-tang area). Propagule input from the outside tends to vary widely and plays a lesser role the farther away a plot is from protection and buffer zones.

Consequently, the number of saplings that disappeared during backwards simulation in the 1st and 2nd year after clear-felling is due to natural regeneration on the site plus (to a lesser extent) former propagule input from the outside.

Supplemental replanting with nursery-grown seedlings aged 1.5–2 years, sized at a diameter at ground of about 3 cm and a height of about 70 cm takes also place in the 2nd year. It is assumed that those seedlings reach sapling stage one to two years later. Accordingly, the number of saplings that disappeared during this phase is due to replanting plus former propagule input from the outside.

Afterwards a time period follows in which only input from the outside is effective and disappearance rates drop thus to the lowest level. Plot-wise natural regeneration, replanting and later on generative reproduction totals can be adjusted by subtracting the propagule input obtained for a plot during this period.

Later on, rising disappearance rates are due to generative reproduction by the young trees. The parameter D is then derived by minimizing the deviation between offspring production rates and sapling disappearance rates via GA optimization.

Srivastava and Khamis (1978) further report that Bruguiera parviflora seedlings/saplings were uniformly distributed and that 3.6% of them had already reached a height of 1.52–3.05 m 12 months after clear-felling. This percentage increased to 60% 12 months later. Thus, the above technique can be readily applied to derive a species-specific parameter D for *Bruguiera gymnorhiza* by accounting for the absence of replanting for this species and by additionally assuming that this species behaves like *B. parviflora*.

As part of the recruitment, localized dispersal around parental trees is simulated as follows: We assume that flowers are primarily produced by terminal branches. Thus, propagules are released exclusively from random x,y-coordinates on the crown margin of a parental tree. After landing on the water surface at the x,y-position of release, a propagule is transported forward by water in steps of 1 m in the direction of the water current that is randomly chosen from 0° to 360° for each propagule. The specific behavior is defined by the following equation:

$$Pos(x, y)_{n+1} = \begin{cases} if \ x \leq P_{spread} \rightarrow Pos(x, y)_n + \vec{u} \\ if \ x > P_{spread} \rightarrow Pos(x, y)_n \end{cases} \tag{10}$$

such that $Pos(x,y)_{n+1}$ is the x,y-position of a propagule at step $n+1$, x is a random number taken from a uniform distribution defined over the closed interval [0, 1], $P_{spread} = 0.9$ represents the probability of spreading considered to be specific to the genus *Rhizophora* (1 parameter), and $\vec{u}$ is a unit vector pointing in the direction of the water current. The dispersal pattern established by this routine mimicks a negative exponential kernel (Levin et al., 2003) which is uniform in all directions.

With the parameter given above the mean and maximum dispersal distances of 100 propagules were measured as 9.09 m and 39.91 m, respectively. In principle, the simulated dispersal distances are in good qualitative agreement with recent findings on species of the *Rhizophora* genus. The majority of *Rhizophora mucronata* propagules remained in 20 m vicinity of the parental tree and only few were carried more than 65 m away (Chan and Husin, 1985;Sengupta et al., 2005). In release experiments carried out by van der Stocken et al. (2015) more than 50% of the *R. mucronata* propagules were recovered at distances less than 20 m and only 1% were recovered at distances of more than 90 m. In a further study Sousa et al. (2007) recovered all painted *R. mangle* propagules within a distance of 8.0 m four weeks after release.

Self-planting is the first mechanism likely to be responsible for the observed short dispersal distances (van Speybroeck, 1992; Cannicci et al., 2008; Dahdouh-Guebas et al., 2011). With the given probability of spreading we assume a self-planting probability of 10% here. By this, we take an intermediary position between researchers that claim a preponderance of self-planting (van Speybroeck, 1992) and those who state it is a rare event (Tomlinson, 1994). Further mechanisms that were made responsible for the short-distance dispersal of *Rhizophora mucronata* propagules are the dense aerial root network acting as a physical barrier and the elongated propagule shape, whereas wave action and water flow velocity were identified as important antagonists in the flume tank experiments of van der Stocken et al. (2015).

Moreover, Wolanski (2017) reports that transport of mangrove propagules occurs mainly during a short period of peak tidal currents and that the net movement of propagules is seaward, because the peak current speed is larger at ebb tide than at flood tide. Based on the dispersal distances of *R. apiculata* propagules referred to above and given the homogenous distribution of trees belonging to this species in the surrounding the plot size of 10 m × 10 m is far too small to study the anisotropy of propagule dispersal and, thus, the dispersal algorithm ignores it at present. This model limitation could be overcome by adding a seaward-directed current vector to our routine. The length of this current vector ought to be parameterized using seedling/sapling data from transects that are orthogonal to the nearest shoreline, are about 40 m long and transgress the seaward boundary of the *Rhizophora apiculata* zone.

While we can infer from the smaller propagule size that *Bruguiera gymnorhiza* is farther dispersed than *R. apiculata* (de Ryck et al., 2012; van der Stocken et al., 2015) and should possess thus a higher probability of spreading P_{spread}, information on dispersal distances is still lacking for both species in the literature (Table 1.1 in van der Stocken et al., 2015). Unlike, flotation and viability periods are known for a much wider range of species (Table 1.3 in van der Stocken et al., 2015). Hence, modeling propagule dispersal would be less challenging if we could simulate the lateral water transport in an area by way of an ecosystem model (compare ch. 4). An improved realism including tidal anisotropy of propagule dispersal would be an additional advantage of this approach.

Certainly, propagules of parental trees at the seaward-side or, more generally, propagules that could escape the aerial root network are prone to long-distance dispersal (LDD), but simulating the long tail of the dispersal kernel realistically was not among our objectives here.

Tree mortality: Tree mortality is governed by two parameters: A tree dies when its average stem volume growth rate falls below a threshold $V_{thre, \ mort}$ [m^3] over a time period T_{sust} [years]. The time period T_{sust} over which trees can sustain growth below the $V_{thre, \ mort}$ was set to 31 years in early calibration. This prevented tree death, but correct parameters can be determined later by manually raising $V_{thre, \ mort}$ and lowering T_{sust} until the first tree deaths occur.

Crown plasticity: The sub-model as described by Grueters et al. (2014) is de-activated due to lack of data (2 parameters).

Forest thinning regime (turned off in early calibration): Visual inspecting marked spatial point patterns of tree positions in 15- and 20-year-old plots (after thinning) using the spatstat package in R (Baddeley and Turner, 2005) revealed that the loggers did not apply a thinning from below (Pretzsch, 2009) as there were many differently sized tree pairs at distances below 1 m. We conclude thus, that the regime consists of two "selective thinning from above" events (Pretzsch, 2009) which remove competing dominant trees at a distance of 1.2 m from pre-dominant trees in year 15 and at a distance of 1.8 m in year 19.

This thinning regime is implemented by the following algorithm: We introduce F_{dom}, the dominant fraction of trees on a plot, as a new parameter. From this parameter the number of dominant trees is calculated (e.g. $F_{dom} = 0.25$, number of trees on the plot = 10; $0.25 \times 10 = 2.5$, 2.5 is raised to the nearest integer = > the 3 thickest, dominant trees). We iterate over the list of dominant trees sorted in descending order and let each tree remove thinner trees from this list in case they are less than 1.2 m (or 1.8 m) apart. Because tree felling is defined as "wrong behavior" and punished with a penalty the Genetic Algorithm assigns F_{dom} a value that is suitable and consistent with the observations.

Scheduling sub-models in the "way-back-machine":
The calculation of the competition is scheduled first.

In the first simulation year, eq. (7) is used to calculate the current tree height h (t) based on competition and the given $d_{1.37}$ (t). In all other years, stem height is available from the previous year.

The current stem volume V (t) in [m^3] is then obtained from:

$$V(t) = F \cdot \pi / 4 \cdot d(t)^2 \cdot h(t) \tag{11}$$

where F is the tree form factor assumed to be 0.65 for *R. apiculata*, d(t) is the diameter at 1.37 m height in [m] and h(t) denotes stem height in [m] at t.

Assuming optimal growth, the previous (smaller) diameter $d(t-1)_{opt}$ is determined by finding the root of the function:

$$d(t) - d(t-1)_{opt} - \Delta d / \Delta t = 0 \tag{12}$$

where d(t) is the current (larger) diameter at t and $\Delta d / \Delta t$ is the optimal diameter increment calculated by eq. (6).

In principle, in mesoFON all root finding is done with the BisectionSolver of the Apache Commons Math library.

From the respective $h_{opt}(t-1)$, calculated by using eq. (7), and V_{opt} (t-1) derived from eq. (11) we can calculate. $\Delta V_{opt} / \Delta t = V(t) - V_{opt}(t - 1)$

The stem volume growth is then reduced by competitive and environmental constraints (salinity, phosphorus) using the formula:

$$\Delta V / \Delta t = \Delta V_{opt} / \Delta t \cdot [1 - (comp_{above} + comp_{below})] \cdot f_{red, \ sal} \cdot f_{red, \ P} \tag{13}$$

with all parameters being defined as above.

The previous stem volume V (t-1) is then V(t) - $\Delta V / \Delta t$ and the true

mesoFON calibration for Rhizophora apiculata (Matang Mangrove Forest Reserve, Malaysia)
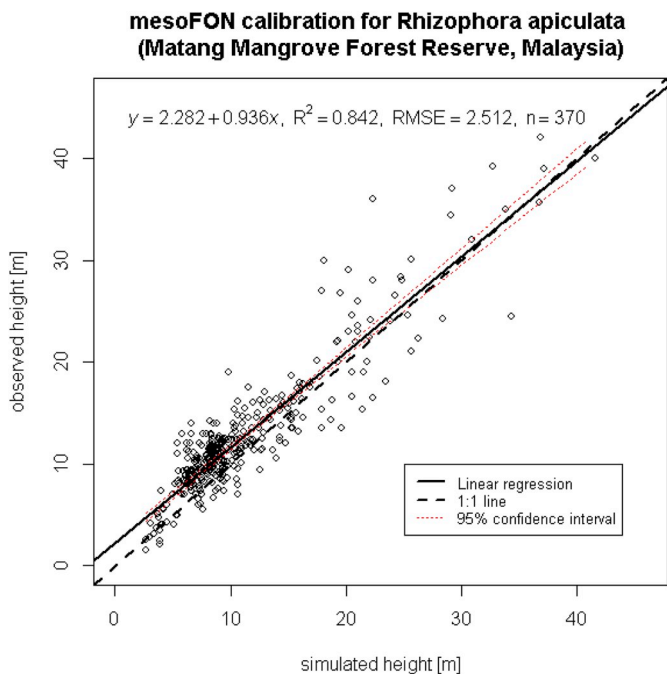

Fig. 4. MesoFON calibration for *Rhizophora apiculata* Bl. In the Matang Mangrove Forest Reserve, Malaysia.

previous (smaller) d(t-1) can be determined by finding the root of the function:

$$V(t-1) - [F \cdot \pi/4 \cdot d(t-1)^2 \cdot h(t-1)] = 0 \qquad (14)$$

where all variables are defined as above and h(t-1) is calculated from eq. (7) and d(t-1).

This completes the scheduling of the sub-models. Altogether, 15 parameters were optimized and 13 were held constant or were turned off. The 36 P levels of the plots were determined by the repair algorithm.

3.2.5. Results of the calibration

Fig. 4 shows the results of the mesoFON calibration for *Rhizophora apiculata*. The best fitness for this run was 8.961 meaning that the average deviation of simulated heights from observed heights was 3.0 m. The data points lie close to the 1:1 line (except for some underestimated large tree heights of plot 8). The linear regression has an intercept of 2.282 m $\pm$ 0.5276 m (95% confidence interval) which does not overlap with 0 and a slope of 0.936 $\pm$ 0.0416 which almost overlaps with 1 (0.978). With 0.842 the R^2 of the regression is substantial.

3.3. The future direction of mesoFON

The direction of future mesoFON development will be determined by operational objectives that follow from chapters 3.2.2 and 3.2.4. In the long run it will be governed by strategic objectives arising out of chapters 2.3.1 and 2.3.2.

The first operational goal is the derivation of (co-)limiting nitrogen and phosphorus functions for *R. apiculata* on the basis of soil NH_4^+, NO_3^- and PO_4^{3-} concentration data and the derivation of a salt tolerance curve for that species based on further salinity measurements. We intend to cross-validate the derived functions with the influence of the soil nutrient status on *R. apiculata* seedling/sapling growth rates obtained by Duarte et al. in The Philippines and Thailand (Fig. 3 in Duarte et al., 1998,). As this data encompasses a broad range of conditions (Duarte et al., 1998) the cross-validation will likely broaden the scope of mesoFON application in Southeast Asia. The second operational goal is the extension of the model to *Bruguiera gymnorhiza*.

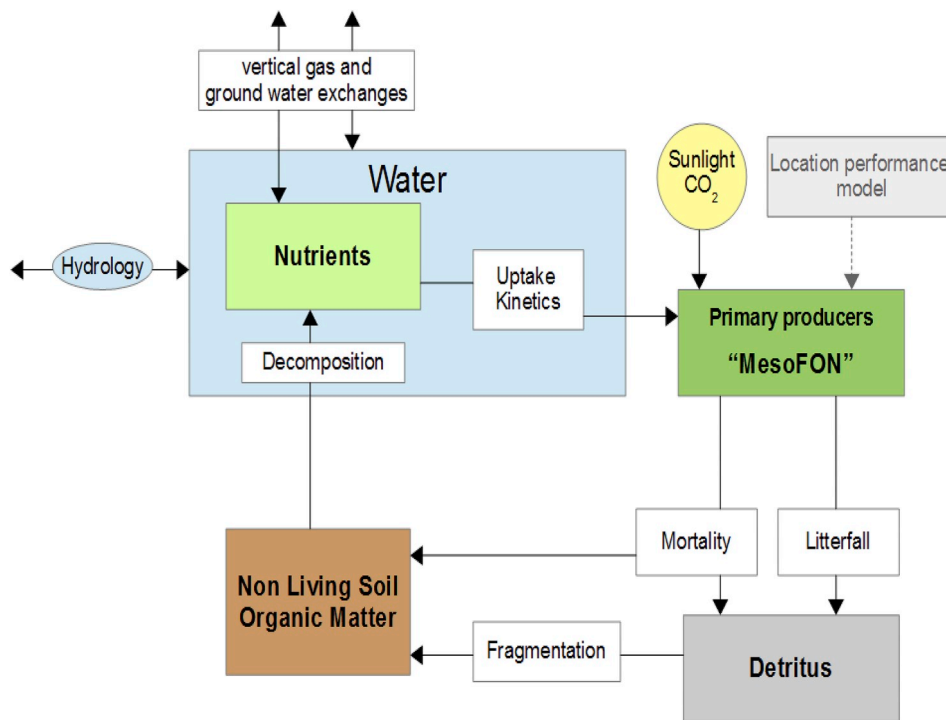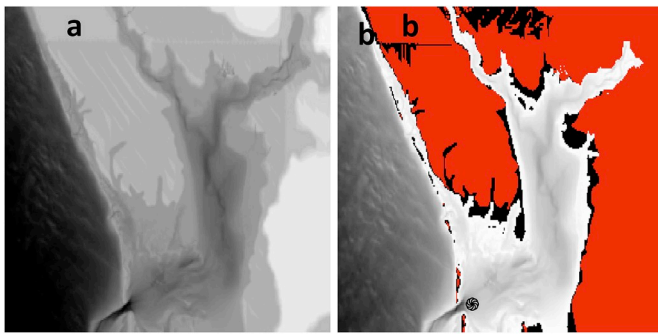Our strategic goal. on the other hand. is to simulate mangroves at

Fig. 5. Overview of state variables and flow processes among sectors in the Genera Ecosystem Model (GEM). Modified from Fitz et al. (1996).

Fig. 6. Simulating a storm surge in the Charlotte Harbor Estuary:
(a) Digital elevation map: Topography and bathymetry
(b) Surface water depth at mean sea level (MSL) with the land area at MSL (in **black**) and the land area at a storm surge of 40.7 cm above MSL measured at Port Boca Grande/Boca Grande Pass (❀) (in **red/grey**). . (For interpretation of the references to colour in this figure legend, the reader is referred to the Web version of this article.)

larger spatial scale and embed mangrove IBMs in ecosystem models, because such IBMbedding will enable the models to mitigate the eutrophication threat and to address the threats of altered hydrology and altered sedimentation. That is why we have begun to make the strategic move with mesoFON into this future direction.

3.4. Ecosystem model selection and porting

In times that were dominated by purely terrestrial ecosystem models (CENTURY, FOREST-BGC, etc.) Fitz et al. (1996) proposed the intriguing idea of a General Ecosystem Model (GEM) applicable to terrestrial and aquatic ecosystems alike. At the time, the model was the final product of the key role mangroves played in ecosystem ecology and ecosystem modeling (Golley et al., 1962; Odum et al., 1974). Later, the GEM formed the basis of the Everglades Landscape Model (ELM, Fitz, 2018). The GEM contains parametrizations for mangrove forests as well as for mangrove scrubs. It is particularly beneficial that this model has been extensively documented (26 research articles; 1 book, Costanza and Voinov, 2005; the homepage, Fitz, 2018).

As a result of this history, we decided to carry out a suitability analysis for embedding an individual-based mangrove growth model in GEM (i.e. IBMbedding) and completed it with very promising results (see Appendix B). The suitability is underlined by the following description of the simulated processes (compare Fig. 5): GEM simulates the sequestration and cycles of carbon, nitrogen and phosphorus in mangrove ecosystems under the influence of surface and subsurface water including lateral transport of water and suspended constituents, such as salt, dissolved inorganic nitrogen (DIN) and phosphorus (DIP), organic matter and sediments. The growth of mangroves and algae, if surface water is present, is controlled by nutrient availability and the hydrological regime. Mangroves have feedback effects on the hydrology via canopy roughness and transpiration. Dead plants, algae and consumers deposit as organic matter, which is decomposed at varying rate dependent on the material's C:N:P ratio and the hydrology. N/P in the organic matter is re-mineralized in that process.

In the meantime, porting the General Ecosystem Model to the agent-based model development framework MASON, GEO-MASON,

Distributed or D-MASON (Luke et al., 2016; Cordasco et al., 2013) has been successfully completed (according to JUNIT tests, JUnit-Team, 2013; Link, 2005). Development in D-MASON allows us to target simulation at larger spatial scale by applying techniques of large-scale distributed agent-based modeling that has been successfully used in other disciplines (e.g. TRANSIMS simulates the traffic of the 7.5 million inhabitants of Switzerland, Helbing and Balietti, 2011). Recently, this so-called macroFON model became ready for the IBMbedding.

3.5. Model testing

As the GEM originally was a unit (single grid) model we had to test the connectedness of the ecosystem cells and to validate the overland water flow among the cells. We chose the Charlotte Harbor Estuary in Southwest Florida for a case study. Because of its tiny mouth the bay represents a benchmark for tidal flow simulations.

To this end, we prepared a topographic/bathymetric map from the U.S. Coastal Relief Model – Florida and East Gulf of Mexico (National Geophysical Data Center, 2001, datum: mean sea level (MSL), cell size: 3 arc-seconds or roughly 90 m) with the help of QGIS (Graser, 2016). Finally, the extracted topographic/bathymetric map of the Charlotte Harbor Estuary, 53 km × 39 km in size at a spatial resolution of 180 m × 180 m was imported into the model via the GeoMason extension (see Fig. 6a).

In the test a storm surge is invoked by only raising the hydraulic head in the cells at the western edge of the map. Fig. 6b shows that the model passed the test qualitatively as the differences between surface water levels at mean sea level and at the storm surge of 40.7 cm above MSL measured at Port Boca Grande/Boca Grande Pass extended far into the Charlotte Bay.

4. Conclusions

We envision that volumes of seawater & amounts of suspended compounds received from the ocean and volumes of freshwater & amounts of suspended compounds from rivers can be measured, whereas community patterns emerge from the horizontal water flows and ecosystem processes in the simulated mangrove ecotone. Community patterns simulated with macroFON are to be compared with remotely sensed patterns to govern the sustainable ecotone management in the Matang Mangrove Forest Reserve.

In the end, this modeling effort will hopefully exemplify how to overcome the ignorance of ecosystem processes in IBMs and the ignorance of plant communities in ecosystem models (Scheiner and Willig, 2011) and help to unify the creek of individual-based modeling with the stream of ecosystem modeling.

Acknowledgements

Appendix A

Table. A1

Interior (anthropogenic & natural), up- and down-stream threats to mangroves for continents/regions and countries (extracted from FAO (2007) & country profiles) along with their drivers and model types suitable for their simulation. Countries, where individual-based models have been applied, are marked in green. Abbreviations are given at the bottom of the table.

Region	Area [km²] (in 2014)	Up-stream Threats	Interior Threats — Anthropogenic Threats	Interior Threats — Natural Threats	Down-stream Threats
Asia	38,195	Shrimp Farms [Eut Poll ◎IBM ◎EM], Agriculture [AltHyd, Eut ◎IBM ◎EM], Urbanization [AltHyd], Tourism [AltHyd], Infrastructure [AltHyd]	Conversion [CF] to Shrimp Farms, Agriculture, Cities, Industry, Tourism, Infrastructure / Over-Exploitation for Charcoal, Fuelwood, Timber [CF GF ◎IBM, ◎FSM]	Typhoons, Cyclones, Storms, Floods [CF GF ◎IBM + MWM]	Urbanization [AltHyd], Infrastructure [AltHyd], Tourism [AltHyd], Sea Level Rise [◎IBM ◎EM]
Indonesia	23,179		Conversion [CF] to Palm Oil Plantations, Salt Pans		Oil Spills [Poll ◎IBM ◎EM]
Malaysia	4,705				
Myanmar	2,522		Conversion [CF] to Rice Paddies		
Philippines	2,061		Conversion [CF] to Salt Pans		
Thailand	1,878				
Bangladesh	1,773				
India	793		Conversion [CF] to Rice Paddies		
Viet Nam	707		Conversion [CF] to Salt Pans, Usage of Agent Orange, Napalm [Poll ◎EM, CF]		
South America	13,689	Industry [Poll ◎EM ◎EM], Domestic Waste Disposal [Poll ◎IBM ◎EM], Dams & River Flow Changes [AltHyd, Sal ◎IBM, Olig ◎IBM, -Sed ◎EM]	Conversion [CF] to (Shrimp Farms)	Hurricanes, Cyclones, Floods [CF GF ◎IBM + MWM]	Sea Level Rise [◎IBM ◎EM]
Brazil	7,665			Cyclones, Storms, Floods [CF, GF ◎IBM + MWM], Climate Change ◎IBM	
Venezuela	2,401		Conversion [CF] to Cities, Tourism	Hurricanes, Floods [CF, GF ◎IBM + MWM]	Urbanization [AltHyd], Tourism [AltHyd], Oil Spills [Poll ◎IBM ◎EM]
Colombia	1,672		Conversion [CF] to Agriculture, Cities, Tourism		Urbanization [AltHyd], Tourism [AltHyd]
Ecuador	936		Conversion [CF] to Salt Pans, Agriculture		
Suriname	510	Runoff from Agriculture: Pesticides [Poll ◎EM]		Cyclones, Storms, Floods [CF GF ◎IBM + MWM]	
Africa	10,761	Agriculture [AltHyd, Eut ◎IBM ◎EM], Urbanization [AltHyd], Infrastructure [AltHyd], Solid Waste Dumping [Poll ◎IBM ◎EM], Sewage Disposal [Poll ◎IBM ◎EM]	Conversion [CF] to Salt Pans, Rice Paddies, (Shrimp Farms), Cities, Construction, Tourism / Over-Exploitation (human pressure) for Fuelwood, Timber, Charcoal [CF GF ◎IBM ◎FSM]	Cyclones, Storms, Floods [CF, GF ◎IBM + MWM], Climate Change [◎IBM]	Urbanization [AltHyd], Infrastructure [AltHyd], Tourism [AltHyd], Sea Level Rise [◎IBM ◎EM]
Nigeria	2,653		Over-Exploitation by Grazing of Camels, Cattle, Goats [◎FSM]		
Mozambique	1,223	Solid Waste Dumping [Poll ◎EM ◎EM]	Over-Exploitation by Grazing of Camels, Cattle, Goats [◎FSM]		
Cameroon	1,113		Over-Exploitation by Grazing of Camels, Cattle, Goats [◎FSM]		Oil Spills [Poll ◎IBM ◎EM]
Gabon	1,081		Over-Exploitation by Grazing of Camels, Cattle, Goats [◎FSM]		
Madagascar	850	Solid Waste Dumping [Poll ◎IBM ◎EM]	Over-Exploitation by Grazing of Camels, Cattle, Goats [◎FSM]		Oil Spills [Poll ◎IBM ◎EM]
North-/Central-America	9,768	Runoff from Agriculture: Fertilizers, pesticides [Eut Poll ◎IBM ◎EM] / Waste Disposal [Poll ◎IBM ◎EM]	Conversion [CF] to Cities, Tourism, Salt Pans, Rice Paddies, Pasture, (Shrimp Farms) / Drainage & Canalization [AltHyd]	Hurricanes, Floods [CF GF ◎IBM]	Urbanization [AltHyd], Tourism [AltHyd], Infrastructure [AltHyd], Sea Level Rise [◎IBM ◎EM]
Mexico	2,987				
Cuba	1,626				
United States	1,556			Climate Change	
Panama	1,323				Oil Spills [Poll ◎IBM ◎EM]
Nicaragua	552				
Oceania	8,464	Tourism [AltHyd], Industry [Poll ◎IBM ◎EM], Waste Disposal [Poll ◎IBM ◎EM]	Conversion [CF] to Tourism, Cities	Cyclones, Storms, Floods [CF GF ◎IBM + MWM]	Urbanization [AltHyd], Tourism [AltHyd], Sea Level Rise [◎IBM ◎EM]
Papua New Guinea	4,170		Over-Exploitation [◎FSM] for Timber, Fuelwood		
Australia	3,315		Conversion [CF] to Tourism, Cities, Infrastructure	Climate Change	
TOTAL	81,575				

Driver Abbreviations: [AltHyd] = Altered Hydrology, [Sal] = Salinization, [CF] = Clear Felling, [GF] = Gap Formation
[Eut] = Eutrophication, [Olig] = Oligotrophication, [Poll] = Pollution, [±Sed] = ±Sedimentation
Model Abbreviations: ◎ IBM = Individual-Based Model (mesoFON), ◎ IBM + MWM = IBM + Mechanistic Windthrow Model, ◎ EM = Ecosystem Model, ◎ FSM = Functional-Structural Model

Appendix B. GEM Suitability Analysis

Summary

The purpose of the General Ecosystem Model (GEM, Fitz et al., 1996) is to simulate the carbon, nitrogen and phosphorus cycles in mangrove ecosystems under the influence of surface and subsurface water including lateral transport of water and suspended constituents, such as salt, dissolved inorganic nitrogen (DIN) and phosphorus (DIP), organic matter and sediments. The growth of mangroves and algae, if surface water is present, is controlled by nutrient availability and the hydrological regime. Mangroves have feedback effects on the hydrology via canopy roughness and transpiration. Dead plants, algae and consumers deposit as organic matter, which is decomposed at varying rate dependent on the material's C:N:P ratio and the hydrology. N/P in the organic matter is re-mineralized in that process.

The General Ecosystem Model (GEM) consists of various sectors each of which is related to a specific set of ecosystem processes. The hydrology

sector of the GEM differentiates among surface water, saturated and unsaturated water in the sediment, the latter being further divided into an aerobic and an anaerobic zone. Horizontal surface water flows are simulated with Manning's equation for overland water flow, while Darcy's equation is used for the simulation of lateral groundwater flows. Major vertical water flows, such as infiltration, percolation and capillary flow, are included. All water flows in the GEM transport inorganic sediment, organic matter, DIN, DIP, salt, algae and consumers with them. Wind- and current-induced hydrodynamics are key controllers of suspension/deposition and consequently of gain or loss of compounds listed above. Primary production results in DIN/DIP uptake from the soil/sediment and is computed separately for mangroves and algae. Mortality from all biotic sectors adds to suspended, deposited organic matter or standing detritus in the GEM. Decomposition subtracts from these organic matter fractions and re-mineralizes N and P. With this backbone, the GEM seems perfectly suitable for the simulation of altered hydrology/sedimentation within the mangrove ecotone.

However, it is currently unclear whether P sorption/desorption in GEM varies with the hydroperiod. Denitrification seems to be strictly anaerobic in GEM, neglecting the coupling of anammox/denitrification with aerobic nitrification. Moreover, we miss a biotic feedback (aerial roots, crab burrows) on the allocation of aerobic vs. anaerobic zones in the soil. In contrast, cyanobacterial N-fixation can be simulated easily via a duplicated N-unlimited algae sector. Thus, GEM seems to be a sound starting point for the simulation of interactions among resource, regulator and hydroperiod gradients in the mangrove ecotone, but the significance of some processes along these gradients has to be clarified or they have to be upgraded otherwise.

Essentially, the conceptual approach to realize the proposed IBMbedding is: Simulate individual mangrove trees with three state variables, i.e. photosynthetic and non-photosynthetic biomass growing as in GEM and trunk biomass growing as in mesoFON. Every light-limitation should exclusively be simulated with FONs. Finally, the state variables of all individuals in the ecosystem model will be aggregated and weighted averaging of parameters therein will be applied.

In this Appendix we provide an analysis of whether the GEM is suitable to simulate the "Eutrophication" and "Altered Hydrology/Sedimentation" drivers of mangrove threats and whether it is suitable for the proposed IBMbedding. The model is divided into process-related sectors whose state variables (or stocks, in System Dynamics Modeling terms) and flow processes are described and whose suitability is evaluated in the following.

In the following we provide details of the various sectors contained in the GEM and discuss its suitability for the embedding of mesoFON.

1. Global Input Sector

Major model inputs are the simulated area, daily precipitation, temperature, air humidity, wind speed and wind direction. Together with latitude and Julian date these inputs are used to compute local solar radiation and monthly cloud cover.

2. Hydrology Sector

GEM differentiates between surface water and unsaturated/saturated water in the soil/sediment pores. Fluxes among these water stocks allow for wet, moist and dry environments. Lateral surface water transport is fast, saturated groundwater flow (below the sediment) is slow in GEM simulations. Other processes accounted for are: infiltration, percolation, evaporation and transpiration of saturated/unsaturated water.

<u>Surface water:</u> Runoff of surface water is scheduled first. The calculation is based on hydraulic head differences among GEM cells using Manning's equation for overland water flow. Runoff therein depends on a roughness coefficient which in turn is controlled by sediment type, vegetation height, tree stem density and water depth. Infiltration of surface water into the unsaturated water zone and replacement of saturated water loss to groundwater by surface water is calculated next. The rest of surface water is available to evaporation under the control of temperature, wind speed and air humidity.

<u>Saturated and Unsaturated Water:</u> Moisture above field capacity percolates from the unsaturated to the saturated zone according to the unsaturated hydraulic conductivity which is reduced with respect to its saturated counterpart. Additional inflow to the saturated zone originates from upward movement of groundwater.

When air within the canopy is decoupled from the atmosphere (as in less dense vegetation, such as forests) transpiration is controlled by canopy stomatal conductance, particularly for water-limited vegetation. Otherwise, it is controlled by physics, namely net radiation, air saturation deficit and wind speed. Roots draw water in part from the unsaturated zone and in part from the saturated zone via capillary flow. Horizontal water flow depends on total water head differences between two cells, accommodates elevation differences thereby, and follows basically Darcy's equation.

Overall, to the best of our knowledge, the hydrology sector complies with current standards (e.g. Jones, 2014) and is thus considered to be still state of the art.

3. Hydrodynamics sector

The sector simulates the transfer of wave energy to shallow water and the shear stress of wave- and current-induced turbulence that drives suspension and deposition of inorganic sediments and organic matter, and affects water clarity. In the process wave dynamics and wave energy are assumed to follow linear wave theory and are computed from wave attributes (height/period/length), fetch within a cell and wind speed.

Along with the hydrology sector this sector seems to fulfill all requirements for the simulation of mangrove threats that have altered hydrology/sedimentation as drivers.

4. Inorganic Sediments Sector

Two state variables are distinguished: Deposited and suspended inorganic sediments. Suspension occurs when the shear stress exceeds a specific mangrove soil resistance in dependence on root density and organic matter in the sediment. Suspended inorganic sediments that enter a cell by water inflow get deposited when the shear stress falls below the mud fluid yield, i.e. the minimum stress at which mud is still kept suspended. Sediment depth changes dynamically due to decomposition of organic matter and suspension/deposition of sediment/soil. In the long run and with a very low constant rate, there is also downwarp of sediment, then being lost from the system.

The sector seems to include all processes required for the simulation of coastal ecosystems such as mangroves.

5. Chemical Constituents Sector

Three constituents are distinguished in the model: salt, inorganic nitrogen and phosphate. Each of them is supposed to be homogeneously distributed in the surface water and the sediment/soil pore water, aggregated in the saturated and unsaturated zone. Al constituents in surface and saturated water are subject to lateral water flows of surface or groundwater. Advective vertical transport and diffusion across the surface water –

sediment/soil water gradient accompanies respective water flows. Generally, a steady state among zones in the sediment/soil is assumed. Loss of saturated water via groundwater flow affects also the unsaturated zone.

Salt Sector: It is realistic that dissolved salt components in the model accompany all water movements described above. This is an invaluable advantage. However, salt is not taken up by the mangroves (generally by the macrophytes sector) in the model. While this assumption is valid with respect to salt-excluding species, it is invalid for salt-excreting species. Wind might blow away salt that has accumulated on the leaves of such species, otherwise leaves filled with salt are transported away via tidal exchange.

Dissolved Inorganic Nitrogen Sector: NH_4^+, NO_2^- and NO_3^- are aggregated into one inorganic nitrogen value. However, the various inorganic nitrogen species are indirectly accounted for, since aerobic and anaerobic sediment zones with their prevailing iredox reactions are differentiated. Nitrogen availability to plants is determined by environmental conditions (e.g. anaerobic sediment, aerobic water column, shallow aerobic sediment surface). N-losses from the sediment water occur by way of denitrification in the anaerobic sediment profile whose extent is determined by processes in the deposited organic matter. This routine does not account for the coupling of denitrification to nitrification which is dependent on oxygen (see Appendix B). The N-releasing anammox reaction, which requires less oxygen, was not known in 1996 and is thus not considered in this GEM version. We have not tested yet, whether the influence of hyroperiod on anammox/denitrification (as proposed in Appendix B) emerges from this routine or not. In any case we miss a feedback of biotic sectors (vegetation via aerial roots and burrows of crabs) on the allocation of aerobic vs. anaerobic sediment zones which is so prominent in mangrove ecosystems (see Appendix B). Nonetheless, inputs of nitrogen to surface water do not take place in GEM, but there is a readily available solution to which we return in the algae sector.

Orthophosphate Sector: Phosphate in the surface water increases from precipitation, from decomposition/mineralization of suspended organic matter (with fixed C:P ratio) and decreases from P uptake of algae, that being a constant fraction of fixed carbon. Similar flows from and to phosphate exist, but they involve mineralization of deposited organic matter and uptake by mangroves (again with a fixed ratio of C fixation and P uptake) instead. Hence, the model ignores that P concentrations in mangrove tissues rise with increasing phosphate availability (compare Appendix B). Similar considerations apply to the dissolved inorganic nitrogen. Sorption and desorption of phosphorus to soil particles in the sediment is included in the model and is dependent on the deposited organic matter stock. Whether this process varies indirectly with the hydroperiod (as proposed in Appendix B) is unclear to us at the moment. Nonetheless, if this is not the case the process could be associated with the anaerobic sediment zone in order to force this dependence (see the DIN Sector above).

In conclusion, these sectors provide a sound starting point for the simulation of interactions among resource, regulator and hydroperiod gradients in the mangrove ecotone. The significance of some processes along these gradients has to be clarified, others have to be upgraded.

6. Algae Sector

According to Fitz et al. (1996) the GEM has only one state variable for algal phytoplankton, but the authors advise to duplicate this sector with some modifications for thee simulation of periphyton dynamics. While the inclusion of a periphyton stock in mangrove ecosystems is not so important, the duplication of the algae sector could be an excellent way to simulate N-fixation by autotrophic cyanobacteria (compare Alongi, 2009 and Appendix B) assuming higher light limitation (because N-fixation is very energy demanding) and absence of N-limitation in the growth control function of this biotic sector.

Algal growth is driven by a maximum growth rate multiplied by the standing stock of alae, a density-dependent feedback (saturating at a maximum algae stock) and the growth control function involving light (integrated over the water depth; light extinction depends on algae, suspended organic matter and sediment in surface water; incident light is affected by shading due to mangrove vegetation, including self-shading) temperature (as usual, a skewed optimum function) and nutrient limitation. GEM assumes a Liebig minimum law of N- and P-limitation and a Michaelis-Menten relationship for each nutrient dissolved in surface water. Given the recent paradigm shift towards N/P co-limitation (Elser et al., 2007, Harpole et al., 2011) alternatively a multiplicative coupling of N/P-effects on growth should be provided in future model versions. Certainly, import and export of algae is associated with horizontal surface water flows. Temperature-dependent respiratory losses of the algal stock are included as well. If the ecosystem dries out all algae die, otherwise a constant algal mortality is set. Unfortunately, this routine seems unlikely to resemble the death of algal blooms due to massive oxygen depletion reported for mangrove ecosystems (???).

7. Macrophytes Sector (= Mangrove Sector)

The marophytes sector contains two state variables, photosynthetic biomass and non-photosynthetic biomass, which differ in their C:N:P ratios and, thus, in their decomposition rates. All species are aggregated in the state variables using weighted averages for parameters. The logic of the growth of the photosynthetic macophyte stock is similar to that of algae, but with some comprehensible modifications: There is also a maximum specific rate of net primary productivity (already reduced by maintenance and growth respiration) multiplied by the stock of the photosynthetic biomass, a density dependence that saturates at the maximum total biomass and a control function that incudes terms for light, air temperature, DIN/ DIP and salt in the sediment and water limitation. Water limitation is a function of soil moisture, depth of the unsaturated zone and rooting depth that ranges between 0 and 1. The principal function of the non-photosynthetic biomass is that of a labile carbon reservoir to/from which C is translocated to match the C:N ratio in photosynthetic biomass with the predefined value. Mortality of the photosynthetic biomass varies with season and water stress, whereas that of the non-photosynthetic part is assumed to be constant.

Concluding, processes involving the photosynthetic component seem sound, but we are skeptical about the lack of explicit allocation to roots as a functional part of the non-photosynthetic macrophyte component and the assumed constant C:N:P ratios. This assumption overestimates carbon fixation with larger N/P supply as that is commonly associated with higher N/P concentrations in plant tissues (compare Appendix B). Nonetheless, in the planned replacement of the macrophyte sector by an individual-based mangrove forest model (= mesoFON) we rely on the following conceptual approach: Each individual tree has three state variables, namely the photosynthetic biomass, the trunk biomass and the non-photosynthetic biomass. The growth of photosynthetic biomass works as described above except for the light limitation which is replaced by the competitive influence of overlapping above-ground FONs. Trunk biomass grows as described for mesoFON with modifications using growth control functions of GEM besides the FON competition. The trunk is assumed to share C:N:P ratios and mortality with the non-photosynthetic component, but does not participate in the translocation process. Aggregated state variables and weighted averages of individual- and species-specific parameters (see above) are used by the ecosystem model (= macroFON) in which mesoFON is embedded. Stem density and height calculations which are used in the hydrological feedback are also weighted according to the total biomass of the individuals

8. Suspended Organic Matter (SOM), Deposited Organic Matter (DOM) and Standing Detritus Sectors

The SOM and DOM stocks comprise dead suspended organic matter along with living decomposers. SOM receives explicit inputs from algae mortality. Additional SOM imports/exports are generated by the suspension/deposition process described above. Photosynthetic and non-photosynthetic macrophyte biomass enters the DOM and the Standing Detritus pools in fixed proportions. All organic matter components are subject to consumption through consumers. DOM and SOM receive inputs from consumer mortality and egestion. Standing detritus exports also to DOM. In all organic matter species decomposition is temperature-dependent. It is retarded when the nitrogen concentration in the respective organic matter falls below a critical value and is carried out at a maximal rate otherwise. In particular, anaerobic and aerobic DOM fractions are decomposed separately and at different rates.

Concluding, the interacting ecosystem processes contained in these sectors seem to be scientifically sound.

We finally complete this suitability analysis with a word of caution: Despite the proposed criticisms and suggestions for improvement the GEM should only be modified after q thorough testing of the model for hidden feedbacks which might produce already desired behavior.

References

Alleman, L.K., Hester, M.W., 2011. Refinement of the fundamental niche of black mangrove (Avicennia germinans) seedlings in Louisiana: applications for restoration. Wetl. Ecol. Manag. 19, 47–60.

Alongi, D.M., 2009. The Energetics of Mangrove Forests. Springer, Dordrecht, pp. 216.

Alongi, D.M., 2012. Carbon sequestration in mangrove forests. Carbon Manag. 3, 313–322.

Baddeley, A., Turner, R., 2005. spatstat: an R package for analyzing spatial point patterns. J. Stat. Softw. 12, 1–42.

Ball, M.C., Cochrane, M.J., Rawson, H.M., 1997. Growth and water use of the mangroves Rhizophora apiculata and R. stylosa in response to salinity and humidity under ambient and elevated concentrations of atmospheric CO2. Plant Cell Environ. 20, 1158–1166.

Ball, M.C., Passioura, J.B., 1994. Carbon gain in relation to water use: photosynthesis in mangroves. In: Schulze, E.-D., Caldwell, M.M. (Eds.), Ecophysiology of Photosynthesis. Springer Berlin Heidelberg, Berlin, Heidelberg, pp. 247–259.

Barik, J., Mukhopadhyay, A., Ghosh, T., Mukhopadhyay, S.K., Chowdhury, S.M., Hazra, S., 2018. Mangrove species distribution and water salinity: an indicator species approach to Sundarban. J. Coast. Conserv. 22, 361–368.

Barr, J.G., DeLonge, M.S., Fuentes, J.D., 2014. Seasonal evapotranspiration patterns in mangrove forests. J. Geophys. Res. Atmos. 119, 3886–3899.

Basyuni, M., Nuryawan, A., Yunasfi, Putri, L.A.P., Baba, S., 2018. Effect of long-term salinity on the growth and biomass of two non-secretors mangrove plants Rhizophora apiculata and Ceriops tagal. IOP Conf. Ser. Earth Environ. Sci. 122, 12042.

Basyuni, M., Wasilah, M., Hasibuan, P.A.Z., Sulistiyono, N., Sumardi, S., Bimantara, Y., Hayati, R., Sagami, H., Oku, H., 2019. Salinity and subsequent freshwater influences on the growth, biomass, and polyisoprenoids distribution of Rhizophora apiculata seedlings. Biodiversitas 20, 288–295.

Berger, U., Hildenbrandt, H., 2000. A new approach to spatially explicit modelling of forest dynamics: spacing, ageing and neighbourhood competition of mangrove trees. Ecol. Model. 132, 287–302.

Berger, U., Rivera-Monroy, V.H., Doyle, T.W., Dahdouh-Guebas, F., Duke, N.C., Fontalvo-Herazo, M.L., Hildenbrandt, H., Koedam, N., Mehlig, U., Piou, C., Twilley, R.R., 2008. Advances and limitations of individual-based models to analyze and predict dynamics of mangrove forests: a review. Aquat. Bot. 89, 260–274.

Botkin, D.B., Janak, J.F., Wallis, J.R., 1972. Rationale, limitations, and assumptions of a northeastern forest growth simulator. IBM J. Res. Dev. 16, 101–116.

Burkhart, H.E., Tomé, M., 2012. Modeling Forest Trees and Stands. Springer Netherlands, Dordrecht.

Burns, B.R., Ogden, J., 1985. The demography of the temperate mangrove [Avicennia marina (Forsk.) Vierh.] at its southern limit in New Zealand. Austral Ecol. 10, 125–133.

Byrne, K.E., 2011. Mechanistic Modelling of Windthrow in Spatially Complex Mixed Species Stands in British Columbia. Ph. D. Thesis. University of British Columbia, Vancouver, Columbia, BC.

Canham, C.D., Finzi, A.C., Pacala, S.W., Burbank, D.H., 1994. Causes and consequences of resource heterogeneity in forests: interspecific variation in light transmission by canopy trees. Can. J. For. Res. 24, 337–349.

Cannicci, S., Burrows, D., Fratini, S., Smith, T.J., Offenberg, J., Dahdouh-Guebas, F., 2008. Faunal impact on vegetation structure and ecosystem function in mangrove forests: a review. Aquat. Bot. 89, 186–200.

Casper, B.B., Jackson, R.B., 1997. Plant competition underground. Annu. Rev. Ecol. Evol. Syst. 28, 545–570.

Chan, H.T., Husin, N., 1985. Propagule dispersal, establishment and survival of Rhizophora mucronata. The Malaysian Forester 48, 324–329.

Chase, J.M., Leibold, M.A., 2003. Ecological Niches. Linking Classical and Contemporary Approaches/Jonathan M. Chase and Mathew A. Leibold. University of Chicago Press, Chicago, London.

Chen, R., Twilley, R.R., 1998. A gap dynamic model of mangrove forest development along gradients of soil salinity and nutrient resources. J. Ecol. 86, 37–51.

Chen, R., Twilley, R.R., 1999. A simulation model of organic matter and nutrient accumulation in mangrove wetland soils. Biogeochemistry 44, 93–118.

Clarke, P.J., Kerrigan, R.A., Westphal, C.J., 2001. Dispersal potential and early growth in 14 tropical mangroves: do early life history traits correlate with patterns of adult distribution? J. Ecol. 89, 648–659.

Cordasco, G., Chiara, R. de, Mancuso, A., Mazzeo, D., Scarano, V., Spagnuolo, C., 2013. Bringing together efficiency and effectiveness in distributed simulations: the

experience with D-Mason. Simulation 89, 1236–1253.

Costanza, R., Voinov, A., 2005. Landscape Simulation Modeling. A Spatially Explicit, Dynamic Approach. Springer, New York, pp. 330.

Crase, B., Liedloff, A., Vesk, P.A., Burgman, M.A., Wintle, B.A., 2013. Hydroperiod is the main driver of the spatial pattern of dominance in mangrove communities. Glob. Ecol. Biogeogr. 22, 806–817.

Dahdouh-Guebas, F., Hettiarachchi, S., Lo Seen, D., Batelaan, O., Sooriyarachchi, S., Jayatissa, L.P., Koedam, N., 2005. Transitions in ancient inland freshwater resource management in Sri Lanka affect biota and human populations in and around coastal lagoons. Curr. Biol. 15, 579–586.

Dahdouh-Guebas, F., Koedam, N., Satyanarayana, B., Cannicci, S., 2011. Human hydrographical changes interact with propagule predation behaviour in Sri Lankan mangrove forests. J. Exp. Mar. Biol. Ecol. 399, 188–200.

Dahdouh-Guebas, F., Verneirt, M., Tack, J.F., van Speybroeck, D., Koedam, N., 1998. Propagule predators in Kenyan mangroves and their possible effect on regeneration. Mar. Freshw. Res. 49, 345.

de Ryck, D.J.R., Robert, E.M.R., Schmitz, N., van der Stocken, T., Di Nitto, D., Dahdouh-Guebas, F., Koedam, N., 2012. Size does matter, but not only size: two alternative dispersal strategies for viviparous mangrove propagules. Aquat. Bot. 103, 66–73.

Deutschman, D.H., Levin, S.A., Devine, C., Buttel, L.A., 1997. Scaling from trees to forests: analysis of a complex simulation model. Sci. Online. http://www.sciencemag.org/site/feature/data/deutschman/index.htm.

Di Nitto, D., Erftemeijer, P.L.A., van Beek, J.K.L., Dahdouh-Guebas, F., Higazi, L., Quisthoudt, K., Jayatissa, L.P., Koedam, N., 2013. Modelling drivers of mangrove propagule dispersal and restoration of abandoned shrimp farms. Biogeosciences 10, 5095–5113.

Doyle, T.W., 1981. The role of disturbance in the gap dynamics of montane rain forest: an application of a tropical forest succession model. In: West, D.C., Shugart, H.H., Botkin, D.B. (Eds.), Forest Succession. Concepts and Application. Springer New York, New York, NY, pp. 56–73.

Doyle, T.W., Krauss, Ken W., Melder, M., Sullivan, J., 2003. SELVA-MANGRO. Integrated landscape and stand-level model of mangrove forest response to sea-level rise and hydrologic restoration of the Everglades, (abstract). In: Best, R., Torres, A.E., Higer, A.L., Henkel, H.S., Mixson, P.R., Eggleston, J.R., Embry, T.L., Clement, G. (Eds.), U.S. Geological Survey Greater Everglades Science Program 2002. Biennial Report. USGS Open-File Report 03-54, Lafayette, LA, USA, pp. 140–141.

Doyle, T.W., Smith III, T.J., Robblee, M.B., 1995. Wind damage effects of Hurricane Andrew on mangrove communities along the southwest coast of Florida, USA. J. Coast. Res. 159–168.

Duarte, C.M., Geertz-Hansen, O., Thampanya, U., Terrados, J., Fortes, M.D., Kamp-Nielsen, L., Borum, J., Boromthanarath, S., 1998. Relationship between sediment conditions and mangrove Rhizophora apiculata seedling growth and nutrient status. Mar. Ecol. Prog. Ser. 175, 277–283.

Duke, N.C., Meynecke, J.-O., Dittmann, S., Ellison, A.M., Anger, K., Berger, U., Cannicci, S., Diele, K., Ewel, K.C., Field, C.D., Koedam, N., Lee, S.Y., Marchand, C., Nordhaus, I., Dahdouh-Guebas, F., 2007. A world without mangroves? Science 317, 41b–42b.

Elser, J.J., Bracken, M.E.S., Cleland, E.E., Gruner, D.S., Harpole, W.S., Hillebrand, H., Ngai, J.T., Seabloom, E.W., Shurin, J.B., Smith, J.E., 2007. Global analysis of nitrogen and phosphorus limitation of primary producers in freshwater, marine and terrestrial ecosystems. Ecol. Lett. 10, 1135–1142.

Eschenbach, C., 2005. Emergent properties modelled with the functional structural tree growth model ALMIS: computer experiments on resource gain and use. Ecol. Model. 186, 470–488.

FAO, 2007. The World's Mangroves 1980-2005. A Thematic Study Prepared in the Framework of the Global Forest Resources Assessment 2005 ix. FAO, Rome, pp. 128.

Faridah-Hanum, I., Latiff, A., Hakeem, K.R., Ozturk, M., 2014. Mangrove Ecosystems of Asia. Springer New York, New York, NY.

Feller, I.C., Friess, D.A., Krauss, K.W., Lewis, R.R., 2017. The state of the world's mangroves in the 21st century under climate change. Hydrobiologia 803, 1–12.

Fernandes, S.O., Dutta, P., Gonsalves, M.-J., Bonin, P.C., LokaBharathi, P.A., 2016. Denitrification activity in mangrove sediments varies with associated vegetation. Ecol. Eng. 95, 671–681.

Fitz, H.C., 2018. ELM. EcoLandMod (ecological landscape modling). http://www.ecolandmod.com.

Fitz, H.C., DeBellevue, E.B., Costanza, R., Boumans, R., Maxwell, T., Wainger, L., Sklar, F.H., 1996. Development of a general ecosystem model for a range of scales and ecosystems. Ecol. Model. 88, 263–295.

Fontalvo-Herazo, M.L., Piou, C., Vogt, J., Saint-Paul, U., Berger, U., 2011. Simulating harvesting scenarios towards the sustainable use of mangrove forest plantations.

Wetl. Ecol. Manag. 19, 397–407.

Gardiner, B., Peltola, H., Kellomäki, S., 2000. Comparison of two models for predicting the critical wind speeds required to damage coniferous trees. Ecol. Model. 129, 1–23.

Godin, C., Sinoquet, H., 2005. Functional-structural plant modelling. New Phytol. 166, 705–708.

Goessens, A., Behara, S., van der Stocken, T., Quispe Zuniga, M., Mohd-Lokman, H., Sulong, I., Dahdouh-Guebas, F., Heil, M., 2014. Is Matang mangrove forest in Malaysia sustainably rejuvenating after more than a century of conservation and harvesting management? PLoS One 9, e105069.

Golley, F., Odum, H.T., Wilson, R.F., 1962. The structure and metabolism of a Puerto Rican red mangrove forest in may. Ecology 43, 9–19.

Graser, A., 2016. Learning QGIS. pp. 210.

Grimm, V., Berger, U., Bastiansen, F., Eliassen, S., Ginot, V., Giske, J., Goss-Custard, J., Grand, T., Heinz, S.K., Huse, G., Huth, A., Jepsen, J.U., Jørgensen, C., Mooij, W.M., Müller, B., Pe'er, G., Piou, C., Railsback, S.F., Robbins, A.M., Robbins, M.M., Rossmanith, E., Rüger, N., Strand, E., Souissi, S., Stillman, R.A., Vabø, R., Visser, U., DeAngelis, D.L., 2006. A standard protocol for describing individual-based and agent-based models. Ecol. Model. 198, 115–126.

Grimm, V., Berger, U., DeAngelis, D.L., Polhill, J.G., Giske, J., Railsback, S.F., 2010. The ODD protocol: a review and first update. Ecol. Model. 221, 2760–2768.

Grimm, V., Railsback, S.F., 2005. Individual-based Modeling and Ecology. Princeton University Press, Princeton, xvi, pp. 428.

Grueters, U., Seltmann, T., Schmidt, H., Horn, H., Pranchai, A., Vovides, A.G., Peters, R., Vogt, J., Dahdouh-Guebas, F., Berger, U., 2014. The mangrove forest dynamics model mesoFON. Ecol. Model. 291, 28–41.

Hamblin, S., Hansen, T., 2013. On the practical usage of genetic algorithms in ecology and evolution. Methods Ecol. Evol. 4, 184–194.

Hamilton, S.E., Casey, D., 2016. Creation of a high spatio-temporal resolution global database of continuous mangrove forest cover for the 21st century (CGMFC-21). Glob. Ecol. Biogeogr. 25, 729–738.

Harpole, W.S., Ngai, J.T., Cleland, E.E., Seabloom, E.W., Borer, E.T., Bracken, M.E.S., Elser, J.J., Gruner, D.S., Hillebrand, H., Shurin, J.B., Smith, J.E., 2011. Nutrient co-limitation of primary producer communities. Ecol. Lett. 14, 852–862.

Helbing, D., Balietti, S., 2011. How to Do Agent-Based Simulations in the Future: from Modeling Social Mechanisms to Emergent Phenomena and Interactive Systems Design, SFI WORKING PAPER: 2011-06-02. Santa Fe Institute, Santa Fe, NM, USA, pp. 56.

Hossain, M.D., Nuruddin, A.A., 2016. Soil and mangrove: a review. J. Environ. Sci. Technol. 9, 198–207.

Hutchison, J., Manica, A., Swetnam, R., Balmford, A., Spalding, M., 2014. Predicting global patterns in mangrove forest biomass. Conserv. Lett. 7, 233–240.

Jones, H.G., 2014. Plants and Microclimate. A Quantitative Approach to Environmental Plant Physiology. Cambridge Univ. Press, Cambridge [u.a.] Online-Ressource (XVII, 407 S.).

JUnit-Team, 2013. JUnit - a programmer-oriented testing framework for Java. http://junit.org/.

Kathiresan, K., Bingham, B.L., 2001. Biology of Mangroves and Mangrove Ecosystems, vol. 40. Elsevier, pp. 81–251.

Kautz, M., Berger, U., Stoyan, D., Vogt, J., Khan, M.N.I., Diele, K., Saint-Paul, U., Triet, T., Nam, V.N., 2011. Desynchronizing effects of lightning strike disturbances on cyclic forest dynamics in mangrove plantations. Aquat. Bot. 95, 173–181.

Kodikara, K.A.S., Jayatissa, L.P., Huxham, M., Dahdouh-Guebas, F., Koedam, N., 2018. The effects of salinity on growth and survival of mangrove seedlings changes with age. Acta Bot. Bras. 32, 37–46.

Krauss, K.W., Lovelock, C.E., McKee, K.L., López-Hoffmann, L., Ewe, S.M.L., Sousa, W.P., 2008. Environmental drivers in mangrove establishment and early development: a review. Aquat. Bot. 89, 105–127.

Krauss, K.W., McKee, K.L., Lovelock, C.E., Cahoon, D.R., Saintilan, N., Reef, R., Chen, L., 2014. How mangrove forests adjust to rising sea level. New Phytol. 202, 19–34.

Kroon, F.J., Kuhnert, P.M., Henderson, B.L., Wilkinson, S.N., Kinsey-Henderson, A., Abbott, B., Brodie, J.E., Turner, R.D.R., 2012. River loads of suspended solids, nitrogen, phosphorus and herbicides delivered to the Great Barrier Reef lagoon. Mar. Pollut. Bull. 65, 167–181.

Lacerda, Luiz D. de, Linneweber, V. (Eds.), 2013. Mangrove Ecosystems. Function and management, pp. 298.

Levin, S.A., Muller-Landau, H.C., Nathan, R., Chave, J., 2003. The ecology and the evolution of seed dispersal. A theoretical perspective. Annu. Rev. Ecol. Evol. Syst. 34, 575–604.

Lewis, R.R., 2005. Ecological engineering for successful management and restoration of mangrove forests. Ecol. Eng. 24, 403–418.

Link, J., 2005. Softwaretests mit JUnit: Techniken der testgetriebenen Entwicklung. dpunkt. Verlag.

Lovelock, C., Feller, I.C., Ball, M.C., Ellis, J., Sorrell, B., 2007. Testing the growth rate vs. geochemical hypothesis for latitudinal variation in plant nutrients. Ecol. Lett. 10, 1154–1163.

Lugo, A.E., 2008. Visible and invisible effects of hurricanes on forest ecosystems: an international review. Austral Ecol. 33, 368–398.

Luke, S., Cioffi-Revilla, C., Panait, L., Sullivan, K., Balan, G., 2016. MASON: a multiagent simulation environment. Simulation 81, 517–527.

Marois, D.E., Mitsch, W.J., 2017. A mangrove creek restoration plan utilizing hydraulic modeling. Ecol. Eng. 108, 537–546.

Meiffert, K. JGAP (c) 2000 - 2018. https://sourceforge.net/projects/jgap/.

Meynecke, J.-O., Richards, R.G., 2014. A full life cycle and spatially explicit individual-based model for the giant mud crab (Scylla serrata): a case study from a marine protected area. ICES (Int. Counc. Explor. Sea) J. Mar. Sci. 71, 484–498.

Mitchell, S.J., Ruel, J.-C., 2015. Chapter 2: modeling windthrow at stand and landscape scales. In: Perera, A.H., Sturtevant, B.R., Buse, L.J. (Eds.), Simulation Modeling of Forest Landscape Disturbances. Springer International Publishing, Cham, pp. 17–44.

Monsi, M., Saeki, T., 1953. Über den Lichtfaktor in den Pflanzengesellschaften und seine Bedeutung für die Stoffproduktion. Jpn. J. Bot. 14, 22–52.

Moorthy, P., Kathiresan, K., 1995. Influence of ntirogen salts on growth and physiological responses of Rhizophora apiculata Blume in non-aerated water culture. Pak. J. Mar. Sci. 4, 133–137.

National Geophysical Data Center, 2001. U.S. Coastal Relief Model - Florida and East Gulf of Mexico. NOAA.

Odum, H.T., Sell, M., Brown, M., Zucchetto, J., Swallows, C., Browder, J., Ahlstrom, T., Peterson, L., 1974. Models of herbicide, mangroves and war in Vietnam. In: The Effects of Herbicides in South Vietnam, Part B: Working Papers. National Academy of Sciences, pp. 302.

Pacala, S.W., Canham, C.D., Saponara, J., Silander Jr., J.A., Kobe, R.K., Ribbens, E., 1996. Forest models defined by field measurements: estimation, error analysis and dynamics. Ecol. Monogr. 66, 1–43.

Pacala, S.W., Canham, C.D., Silander Jr., J.A., 1993. Forest models defined by field measurements: I. The design of a northeastern forest simulator. Can. J. For. Res. 23, 1980–1988.

Pacala, S.W., Deutschman, D.H., 1995. Details that matter: the spatial distribution of individual trees maintains forest ecosystem function. Oikos 74, 357.

Peltola, H., Kellomäki, S., Väisänen, H., Ikonen, V.-P., 1999. A mechanistic model for assessing the risk of wind and snow damage to single trees and stands of Scots pine, Norway spruce, and birch. Can. J. For. Res. 29, 647–661.

Penman, H.L., 1948. Natural evaporation from open water, bare soil and grass. Proc. R. Soc. Lond. 193, 120–145.

Perttunen, J., 2008. The Lignum Functional-Structural Tree Model, vol. 52 Helsinki University of Technology, Espoo [58] s.

Piou, C., Berger, U., Hildenbrandt, H., Feller, I.C., 2008. Testing the intermediate disturbance hypothesis in species-poor systems: a simulation experiment for mangrove forests. J. Veg. Sci. 19, 417–424.

Pretzsch, H., 2009. Forest Dynamics, Growth and Yield from Measurement to Model. Springer, Berlin, London.

Primavera, J.H., 2006. Overcoming the impacts of aquaculture on the coastal zone. Ocean Coast Manag. 49, 531–545.

Rabinowitz, D., 1978. Dispersal properties of mangrove propagules. Biotropica 10, 47.

Rasiah, V., Armour, J.D., Cogle, A.L., 2005. Assessment of variables controlling nitrate dynamics in groundwater: Is it a threat to surface aquatic ecosystems? Marine Pollution Bulletin 51, 60–69. https://doi.org/10.1016/j.marpolbul.2004.10.024.

Reef, R., Feller, I.C., Lovelock, C.E., 2010. Nutrition of mangroves. Tree Physiol. 30, 1148–1160.

Richards, D.R., Friess, D.A., 2016. Rates and drivers of mangrove deforestation in Southeast Asia, 2000–2012. Proc. Natl. Acad. Sci. U.S.A. 113, 344–349.

Robert, E., Schmitz, N., A Kirauni, H., Beeckman, H., Koedam, N., 2009. Salinity fluctuations in the mangrove forest of Gazi Bay, Kenya: lessons to take for future research. Nat. Faune 24, 89–95.

Robertson, A.I., Phillips, M.J., 1995. Mangroves as filters of shrimp pond effluent: predictions and biogeochemical research needs. In: Wong, Y.-S., Tam, N.F.Y. (Eds.), Asia-Pacific Symposium on Mangrove Ecosystems. Springer Netherlands, Dordrecht, pp. 311–321.

Rojas, A., Holguin, G., Glick, B.R., Bashan, Y., 2001. Synergism between *Phyllobacterium sp.* (N2-¢xer) and *Bacillus licheniformis* (P-solubilizer), both from a semiarid mangrove rhizosphere. FEMS Microbiology Ecology 35, 181–187. https://doi.org/10.1111/j.1574-6941.2001.tb00802.x.

Salem, M.E., Mercer, D.E., 2012. The economic value of mangroves: a meta-analysis. Sustainability 4, 359–383.

Sanderman, J., Hengl, T., Fiske, G., Solvik, K., Adame, M.F., Benson, L., Bukoski, J.J., Carnell, P., Cifuentes-Jara, M., Donato, D., Duncan, C., Eid, E.M., Ermgassen, P.z., Lewis, C.J.E., Macreadie, P.I., Glass, L., Gress, S., Jardine, S.L., Jones, T.G., Nsombo, E.N., Rahman, M.M., Sanders, C.J., Spalding, M., Landis, E., 2018. A global map of mangrove forest soil carbon at 30 m spatial resolution. Environ. Res. Lett. 13, 55002.

Sarker, S.K., Reeve, R., Thompson, J., Paul, N.K., Matthiopoulos, J., 2016. Are we failing to protect threatened mangroves in the Sundarbans world heritage ecosystem? Sci. Rep. 6, 395.

Scheiner, S.M., Willig, M.R. (Eds.), 2011. The Theory of Ecology x. The University of Chicago Press, Chicago, London, pp. 404.

Sengupta, R., Middleton, B., Yan, C., Zuro, M., Hartman, H., 2005. Landscape characteristics of Rhizophora mangle forests and propagule deposition in coastal environments of Florida (USA). Landsc. Ecol. 20, 63–72.

Shugart, H.H., 1984. A theory of forest dynamics. In: The Ecological Implications of Forest Succession Models. Springer-Verlag, New York, xiv, pp. 278.

SORTIE-ND, (c), 2001-2017. Software for Spatially-Explicit Simulation of Forest Dynamics. SORTIE-ND.

Sousa, W.P., Kennedy, P.G., Mitchell, B.J., Ordóñez, L.B.M., 2007. Supply-side ecology in mangroves: do propagule dispersal and seedling establishment explain forest structure ? Ecol. Monogr. 77, 53–76.

Spalding, M., Kainuma, M., Collins, L., 2011. World Atlas of Mangroves. Taylor and Francis, Hoboken, pp. 336.

Srivastava, P.B.L., Khamis, D., 1978. Progress of natural regeneration after final felling under the current silvicultural practices in Matang mangrove reserve. Pertanika 2, 126–135.

Strigul, N., Pristinski, D., Purves, D.W., Dushoff, J., Pacala, S.W., 2008. Scaling from trees to forests: tractable macroscopic equations for forest dynamics. Ecol. Monogr. 78, 523–545.

Taillardat, P., Friess, D.A., Lupascu, M., 2018. Mangrove blue carbon strategies for climate change mitigation are most effective at the national scale. Biol. Lett. 14.

Tomlinson, P.B., 1994. The Botany of Mangroves, vol. vol. III. Cambridge University Press, Cambridge, pp. 419.

Twilley, R.R., 2009. Ecogeomorphic models of nutrient biogeochemistry for mangrove wetlands. In: Perillo, Gerardo M.E. (Ed.), Coastal Wetlands. An Integrated Ecosystem Approach. Elsevier, Amsterdam, Boston, pp. 641–682.

Twilley, R.R., Chen, R., 1998. A water budget and hydrology model of a basin mangrove forest in Rookery Bay, Florida. Mar. Freshw. Res. 49, 309.

Twilley, R.R., Rivera-Monroy, V.H., 2005. Developing performance measures of mangrove wetlands using simulation models of hydrology, nutrient biogeochemistry, and community dynamics. J. Coast. Res. 79–93.

Valiela, I., Bown, J.L., York, Joannea K., 2001. Mangrove forests: one of the world's threatened major tropical environments. Bioscience 51, 807.

van der Stocken, T., Ryck, D.J.R. de, Vanschoenwinkel, B., Deboelpaep, E., Bouma, T.J., Dahdouh-Guebas, F., Koedam, N., 2015. Impact of landscape structure on propagule dispersal in mangrove forests. Mar. Ecol. Prog. Ser. 524, 95–106.

van Speybroeck, D., 1992. Regeneration strategy of mangroves along the Kenya coast: a first approach. Hydrobiologia 247, 243–251.

Ventana Systems Inc, 2015. Allocation by Priority. (c). http://vensim.com/allocation-by-priority-alloc-p/.

Vincent, G., Harja, D., 2007. Exploring ecological significance of tree crown plasticity through three-dimensional modelling. Ann. Bot. 101, 1221–1231.

Vogt, J., Piou, C., Berger, U., 2014. Comparing the influence of large- and small-scale disturbances on forest heterogeneity: a simulation study for mangroves. Ecol. Complex. 20, 107–115.

Vovides, A.G., Vogt, J., Kollert, A., Berger, U., Grueters, U., Peters, R., Lara-Domínguez, A.L., López-Portillo, J., 2014. Morphological plasticity in mangrove trees: Salinity-related changes in the allometry of *Avicennia germinans*. Trees 28, 1413–1425. https://doi.org/10.1111/j.1365-2745.2012.02019.x.

Watson, J.G., 1928. Mangrove forests of the Malay Peninsula. Malayan forest records – no. 6 Fraser & Neave, 275.

Weiskittel, A.R., 2011. Forest Growth and Yield Modeling. Wiley-Blackwell, Chichester, pp. 415 (Seiten.).

Wolanski, E., 2017. Bounded and unbounded boundaries – untangling mechanisms for estuarine-marine ecological connectivity: scales of m to 10,000 km – a review. Estuarine. Coast Shelf Sci. 198, 378–392.

Wolanski, E., Elliott, M., 2015. Estuarine Ecohydrology. An Introduction. Elsevier, pp. 332.

Yeniay, Ö., 2005. Penalty function methods for constrained optimization with genetic algorithms. MCA 10, 45–56.